NOVEL LOW SHRINKAGE THERMOPLASTIC OLEFINS WITH COOL PIGMENTS ADDITIVES: DESIGN, PREPARATION AND PERFORMANCE EVALUATION

by

Çağla Girişken

Submitted to the Graduate School of Engineering and Natural Sciences

in partial fulfillment of the requirements for the degree of

Master of Science

SABANCI UNIVERSITY

July 2021

NOVEL LOW SHRINKAGE THERMOPLASTIC OLEFINS WITH COOL PIGMENTS ADDITIVES: DESIGN, PREPARATION AND PERFORMANCE EVALUATION

Approved by:

[redacted]

[redacted] approval: July 05, 2021

To my loved ones.

ABSTRACT

NOVEL LOW SHRINKAGE THERMOPLASTIC OLEFINS WITH COOL PIGMENTS ADDITIVES: DESIGN, PREPARATION AND PERFORMANCE EVALUATION

Çağla GİRİŞKEN

Materials Science and Nanoengineering, MSc. Thesis, 2021

Thesis Supervisor: Prof. Dr. Yusuf Ziya Menceloğlu

Keywords: Cool black surface, cool black pigments, thermoplastic polyolefins, plastomers, low mold shrinkage, automotive industry

Energy consumption due to the excessive use of air conditioning especially in hot summer days, in buildings and vehicles is one of the most important considerations about environmental health. Particularly, the heat accumulated in the inner black parts used in vehicles due to the absorbed solar light highly contributes to the use of excessive air conditioning and causes the overheating inside the vehicle. Thermoplastic olefins (TPOs) is the most commonly used polymeric material in automotive industry, in these inner parts such as trim and dashboards, due to their better elastomeric properties. Another challenging problem during the production of these materials is to control the mold shrinkage of TPOs since these parts have very high aspect ratio. So, this thesis treats these two problems and try to find an optimum combined solution. The aim is to obtain thermoplastic olefin materials having black color with cool surface and low mold shrinkage. Therefore, first part of the thesis engaged in preparation of TPO formulations with low mold shrinkage by melt blending plastomers which have various physical/mechanical properties into a polyolefin phase. As a result of the structure-function relationship study of plastomers, the TPO material with lowest mold shrinkage is obtained with the incorporation of plastomer having lowest crystallinity. Then, second part of the thesis focused on generation of cool black surface by incorporation of cool black pigments which have near-infrared (NIR) reflective and transparent properties into the formulation of TPO material with lowest mold shrinkage. After evaluation of surface temperature, reflectance and physical/mechanical properties, MIX_5 is considered as the optimum TPO compound having 28.5% decrease in surface temperature compared to conventional black pigments and with mold shrinkage values in parallel (0.61%) and perpendicular (0.11%) to flow direction.

ÖZET

SOĞUK PİGMENT KATKI MADDELİ, DÜŞÜK KALIP ÇEKMELİ YENİ TERMOPLASTİK OLEFİNLER: TASARIM, HAZIRLAMA VE PERFORMANS DEĞERLENDİRMESİ

Çağla GİRİŞKEN

Malzeme Bilimi ve Nanomühendisliği, Master Tezi, 2021

Tez Danışmanı: Prof. Dr. Yusuf Ziya Menceloğlu

Anahtar Kelimeler: Soğuk siyah yüzey, soğuk siyah pigmentler, termoplastik poliolefinler, plastomerler, düşük kalıp çekmesi, otomotiv endüstrisi

Günümüzde çevre sağlığına tehdit oluşturan en önemli etmenlerden biri özellikle yaz günlerinde bina ve arabalarda aşırı klima kullanımından kaynaklanan enerji tüketimidir. Özellikle uzun süre güneş altında bekleyen arabaların iç kısımlarında kullanılan siyah parçalar tarafından emilen güneş ışığı arabanın iç ısısını çok arttırmakta ve aşırı klima kullanımını neden olmaktadır. Diğer poliolefin malzemelere oranla daha iyi elastomerik özellikler gösteren Termoplasitk olefinler (TPO), arabaların iç kısımlardaki ön konsol, gösterge paneli ve torpido gibi alanlarda kullanılan en yaygın polimer malzemedir. Bu malzemelerin üretimi sırasında karşılaşılan en önemli zorluklardan biri, TPO'ların kalıp çekmesini kontrol etmektir çünkü bu parçalar çok yüksek en-boy oranına sahiptir. Bu nedenle, bu tez bahsi geçen iki sorunu ele almakta ve ortak ideal bir çözüm aramaktadır. Tezin amacı, düşük yüzey sıcaklığı ve kalıp çekmesine sahip siyah renkli termoplastik olefin malzemeler elde etmektir. Bu nedenle, tezin ilk bölümünde, çeşitli fiziksel / mekanik özelliklere sahip plastomerlerin bir poliolefin faz içerisine eritilerek karıştırılmasıyla düşük kalıp çekmesine sahip TPO malzemelerinin hazırlanmasını üzerine çalışılmıştır . Plastomerlerin yapı-fonksiyon ilişkisi çalışması sonucunda, en düşük kristalleşme derecesine sahip plastomerin katılmasıyla en düşük kalıp çekmesine sahip TPO malzeme elde edilmiştir. Tezin ikinci bölümünde ise, yakın kızılötesi (NIR) ışınları yansıtıcı ve geçirici özelliklere sahip soğuk siyah pigmentlerin, en düşük kalıp çekmesine sahip TPO malzeme formülüne katılmasıyla soğuk siyah yüzeye sahip TPO malzemeler oluşturmaya odaklanmıştır. Yüzey sıcaklığı, yüzeyden yansıma ve fiziksel/mekanik özelliklerin değerlendirilmesinden sonra, MIX_5, geleneksel siyah pigmentlere göre yüzey sıcaklığında %28,5 düşüş ve akışa paralel ve dik yönlerde sırasıyla % 0,61 ve %0,1 değerlerinde kalıp çekmeye sahip optimum TPO bileşiği elde edilmiştir.

ACKNOWLEDGEMENTS

First of all, I would like thank to my advisor Prof. Dr. Yusuf Ziya Menceloğlu and my co-advisor Osman Gökhan Ersoy for their patient and sincere guidance, advices and motivation.

I would like to thank also my thesis committee members Prof. Dr. Canan Atılgan, Prof. Dr. İbrahim Kürşat Şendur, Assoc. Prof. Dr. Fevzi Çakmak Cebeci and Prof. Dr. İbrahim Ersin Serhatlı for their valuable contributions and supports.

Very special thanks to all my research group members at Sabancı University, especially to Merve Senem Seven and Yeşim Menceloğlu for their friendly support and help during my studies in laboratory and thesis preparation. Also, I am very thankful to all faculty members of Material Science and Engineering Program and Burçin Yıldız for their helps and supports.

Furthermore, I have special thanks to individually to all members of Ravago Petrochemical Company production team, R&D laboratory technicians and my co-workers; Beste Pamukoğulları Acar, Başak Başar, Buse Ergene, Zafer Kol and Halil Yalçın for their endless help, support and motivation.

I have also very special thanks to İlayda Berktaş, my M.Sc. study partner, a priceless friend and a sincere patient supporter and motivator during all my studies and rest of all the valuable time spent together.

Finally and most importantly, the greatest thanks go to my family for their unconditional support, encouragement and motivation throughout my studies and all my life.

TABLE OF CONTENTS

LIST OF FIGURES

LIST OF TABLES

LIST OF ABBREVIATIONS

CB	Carbon Black
DSC	Differential Scanning Calorimetry
FTIR	Fourier-Transform Infrared
MD	Molecular Dynamic
MFI	Melt Flow Index
NIR	Near Infrared
MB	Masterbatch
MIX	Mixture
NMR	Nuclear Magnetic Resonance
PP	Polypropylene
PPH	Homopolymer polypropylene
PPC	Copolymer polypropylene
REF	Reflective
R_g	Radius of Gyration
SEM	Scanning Electron Microscopy
Ti	Titanium dioxide
TPO	Thermoplastic olefin
TRANS	Transparent
UV	Ultraviolet
VIS	Visible
XRF	X-Ray Fluorescence

CHAPTER 1

1.State of Purpose

Climate change and deterioration of microclimate in urban areas pose serious threats for human and environmental health since they lead to global warming. The heat accumulated in the atmosphere causes higher temperature increase in urban areas, especially in hot summer days, which leads to overuse of air conditioning at indoor space such as buildings and vehicles. Due to that excessive use, air conditioning is responsible for the 30–50% of the total electric energy consumption [1,2]. Especially, air conditioning usage in vehicles, which are exposed to sunlight for a long period of time in hot summer days, is inevitable. Increasing population, traffic volume and the time spent in traffic create need of comfort which results in constantly working air conditions [3]. Beyond the comfort, health and safety of the driver is strongly depends on the vehicle indoor environment temperature and humidity. So, the air conditioning used in vehicles significantly causes a serious energy consumption [4].

Indoor temperature increase in vehicles is commonly caused by the absorbed sunlight heat by the black or dark colored inside plastic parts such as dashboards, door panels and arm set etc. Since these parts should have black or dark color in order to prevent the distraction of the driver because of the reflecting sunlight if these parts have white or light color. However, these parts, having black color, absorb the heat as well as the light coming from the sun, cause over heating of the cabin and encourage use of air conditioning. So, as represented in Figure 1, a possible solution for this problem can be considered as obtaining cool black surface which absorbs the visible light region of the light spectrum for black color view but reflects the NIR region of the light spectrum which is responsible for heating. Since the NIR region corresponds to higher wavelength of the light spectrum, it has lower energy which decreases the motion of particles. Due to that property, NIR dissipates it’s energy in the form of heat. Also, NIR region having the highest percentage in the sunlight spectrum, it highly contributes to the temperature rise [5].

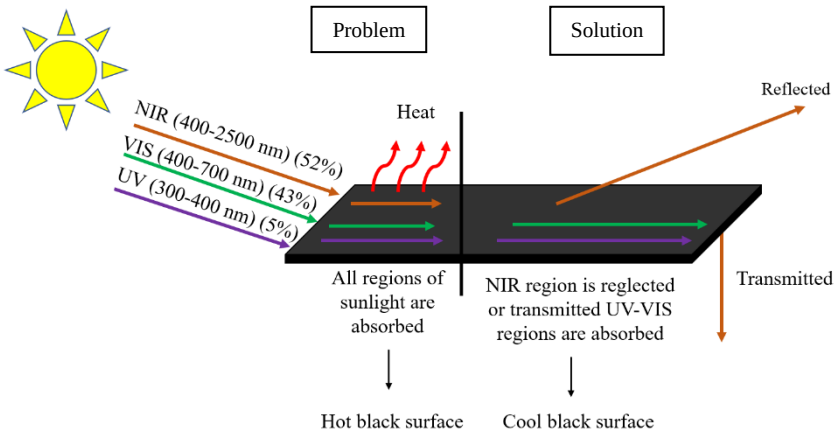

Figure 1. Schematic representation of possible solution for surface heating of black parts

Another problem about these inner parts of the vehicles lies in their production period. Thermoplastic olefins (TPOs), having better elastomeric properties, are the most commonly used polymeric materials for the production of these parts. However, since these parts have very high aspect ratio, controlling their mold shrinkage during the production is one of the most challenging problems in automotive industry [6,7].

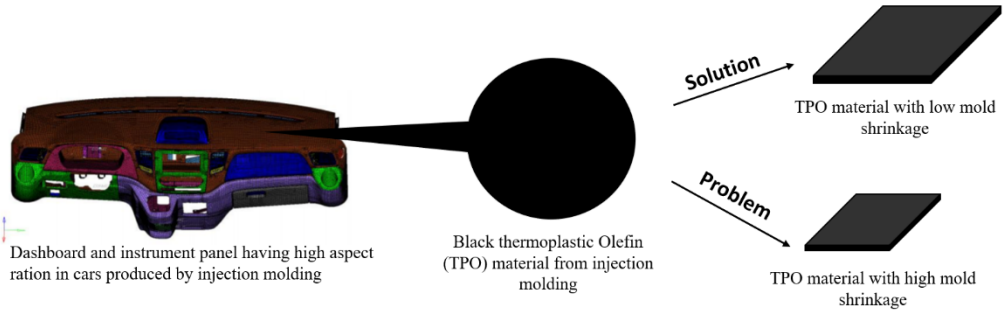

Figure 2. Schematic representation of mold shrinkage in automotive inner parts [8]

So, this thesis treats these two problems and try to find an optimum combined solution. Therefore, the aim of the thesis is to create TPO materials having cool black surface with low mold shrinkage. In line with this purpose, this thesis is composed of two major parts where the first part involves the preparation of TPO formulations with low mold shrinkage and the second part treats the incorporation of cool black pigment fillers into the TPO material with low mold shrinkage values in order to obtain cool black surface.

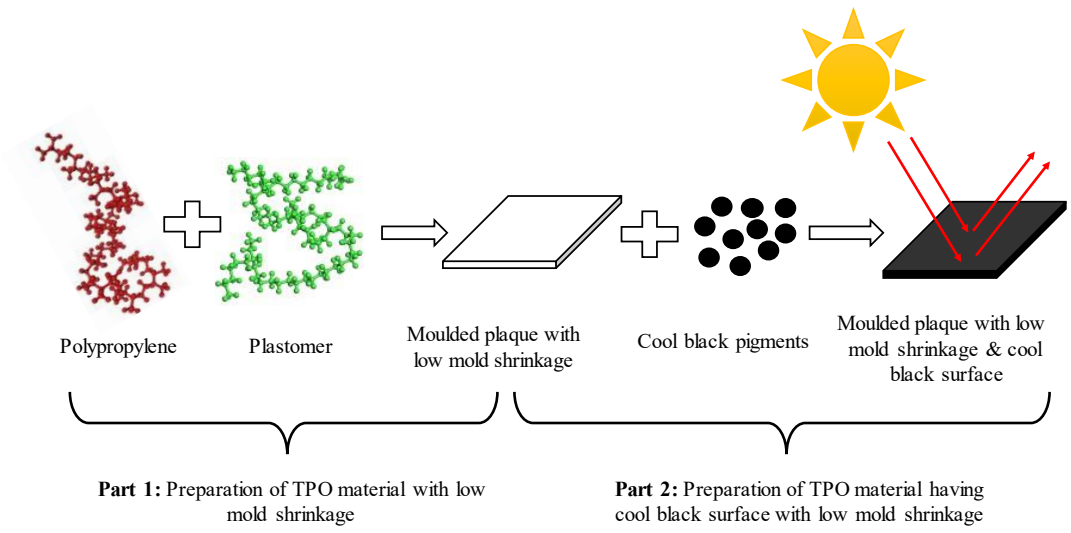

Figure 3. Schematic representation of progressive production of TPO materials having cool black surface with low mold shrinkage

As represented in Figure 3, the first part of the thesis is the production of TPO material with low mold shrinkage. Since TPOs are composition of a polyolefinic and an elastomeric phase, polypropylene (PP) was used as polyolefinic phase and plastomers were used as elastomeric phase. Based upon the idea that morphology of polymers can effect their final functions and properties, TPO formulations were genererated by incorporation of plastomers having different physical, mechanical and morphological properties and compounded with polypropylene by melt mixing method. Prior to compounding, structural analysis of plastomers were conducted in order to observe the effect of plastomer structure on the functions and properties of the final TPO material, especially on mold shrinkage. Then, in the second part, cool black pigment incorporation into previously obtained TPO material wtih low mold shrinakge was realised. Two types of cool black pigments, which are NIR reflective and NIR transparant, were investigated. Their surface temperature and reflectance behaviors in TPO material were compared to the those of TPO materials with conventional pigments such as carbon black which is used due to its best black color in industry and titanium dioxide which is mostly preffered due to its white color and best reflectance values. Comparison with compounds having carbon black showed the recovery at the surface temperature and reflectance values despite to a black colored material and comparison with compounds having titanium dioxide showed at which extent the black materials' properties approached to the values of white materials which are considered as the best. In addition to surface temperature

and reflectance measurements, mechanical properties and mold shrinkage of the TPO compounds with were also studied.

As a result of these two studies, an optimum compound having low mold shrinkage and cool black surface was obtained.

First part of this thesis has been published in the following form and the second part is under preparation or submission process:

Girişken Ç. Avaz Seven S. Ersoy O.G. Menceloğlu Y.Z. Investigation of Structure-Morphology-Function Relationship of Plastomers Used to Produce Low Mold Shrinkage Thermoplastic Olefins. European Polymer Journal.

CHAPTER 2

2. Investigation of Structure-Morphology-Function Relationship of Plastomers Used to Produce Low Mold Shrinkage Thermoplastic Olefins

2.1. Introduction

Thermoplastic Polyolefins (TPOs) are a type of thermoplastic elastomers (TPEs) containing a polyolefin thermoplastic component such as polypropylene (PP) or polyethylene (PE) and an olefin copolymer such as rubber, elastomer, plastomer etc. [9]. Also, additives such as talc, fiberglass, carbon fiber, oil or pigments can be incorporated in TPOs in order to obtain desired mechanical and thermal properties. Compounding of these materials yields a multiphase structure where the polyolefin thermoplastic part is the continuous matrix that ensures tensile strength and rigidity whereas the olefin copolymer and the additive parts are the dispersed components which impart elastomeric properties such as flexibility, resilience and toughness [9,10].

Application areas of TPOs are automotive industry, roofing and etc. due to their flexible structures and easy processability by injection molding [11]. Particularly, TPOs are commonly used as bumper covers, exterior fascia, air dams and other trim, dashboard skins and airbag covers in automotive industry [9,12,13]. Especially dashboards combining many components and providing structural integrity to the vehicle, the dimensional stability, mold shrinkage and mechanical performances of TPOs used in these parts are very important. Most of the automotive specifications state that the mold shrinkage values should not exceed 0.8-1.2% and the minimum values should be for mechanical properties such as tensile strength at 10 MPa, elongation value at 350-400% and hardness values between 56-65 shore D [14,15,16]. So, the challenge in production of these parts is to obtain low mold shrinkage while keeping required mechanical properties [13,17]. For instance, TPO materials targeted to be used in the automotive parts like bumpers, body panels, dashboards, and door claddings, were studied by Grestenberger et al. who prepared PP/EPR blends as TPO materials targeting to investigate the effect of phase morphology on the mold shrinkage of plates. However, the mold shrinkage values were not managed to be reduced under 1% [18].

As dispersed elastomeric part, plastomers can be used in TPO compounds since they provide additional advantages than elastomers. They carry both the rubber like property of elastomers and the ease of processability of plastics. Plastomers contain considerably amorphous phases in their structure with low crystallinity which originate from the destruction of the inherent crystallinity of dominant monomer by addition of another monomer in minor amounts leading to amorphous segments along the polymer chain [19]. Addition of minor monomers such as octene or butene into the structure of dominant phase of ethylene, ensures the increase in amorph phase of plastomers since they change the branching or packing properties of the plastomers. These structural modifications lead to decrease in crystallinity and hence provide lower mold shrinkage of the final product [20]. Thus, the function and properties of final TPO product is highly dependent on the morphology and molecular structure of the incorporated plastomers.

One of the best tools to identify the relationship between the structure, morphology and function of polymers is to conduct their computational studies such as molecular dynamic (MD) simulations. Since they provide the opportunity to understand the crystallization behavior of chain molecules in polymer systems, they can be considered as a promising tool because physical and mechanical properties of crystalline polymers are controlled by their crystal structures, degrees of crystallinity, and morphologies [21]. The information such as molecular trajectories, chain length, chain folds, side chains and branching obtained from MD simulation ensure a better understanding of crystalline structure of a polymer [22]. For instance, the study conducted by Avaz et al. investigate the effect of soft segment chain length on the morphology of PEO based poly(urethane urea) copolymers with the help of MD simulations and found that the relation between the structure and property of copolymer is controlled by a critical chain length [23]. Also, Yang et al. treats the effect of side chain groups on crystallinity by conducting the MD simulations of polyethylene/fullerene (PE/C60) nanocomposites containing various fullerene contents as side groups and observed that increasing C60 content decreases the crystallinity of PE/C60 nanocomposites [24].

In this part of the thesis, the main objective is to develop the optimum TPO formulation(s) with low mold shrinkage and required physical and mechanical properties because it is one of the most challenging problems in automotive industry since the parts having very high aspect ratio such as bumper, exterior trims, glass run channel are produced by those materials [25].

In the light of this purpose, major reasons for mold shrinkage were considered as the effect of elastomeric content load in TPO formulations, in this case the plastomer load, effect of the crystallinity of incorporated plastomer and the effect of flow (MFI) property of plastomer. So, prior to compounding, structural analysis and MD simulation studies were conducted in order to investigate the structural mechanism of plastomers which affect the properties of final TPO products formulated with these plastomers. Then TPO compounds were prepared by incorporation of plastomers having different tensile strength, melt flow index (MFI), hardness and crystallinity which is the most important and the determinant parameter for the mold shrinkage. Mechanical and thermal test results were studied.

2.2. Experimental Process

2.2.1. Materials

Copolymer polypropylene (PPC) which was used as thermoplastic polyolefin component, named ISPLEN™ PB 180 G2M was supplied from Repsol Company. It has 20 g/10min. MFI, 25 MPa tensile strength and 60 Shore D hardness values. Plastomers having same chemical formula, ethylene-1-octene, with different properties such as octene content, crystallinity, hardness, melt flow index (MFI) and tensile strength and elongation at break were chosen from Engage series supplied by Dow Chemicals Company. Properties of four chosen plastomers, incorporated in TPO formulations, are represented in Table 1.

Table 1. Properties of plastomers used in TPO formulations [26,27,28,29]

Property	**Engage 8100**	**Engage 8540**	**Engage 8842**	**Engage 8407**
Density (g/cm³)	0.87	0.90	0.85	0.87
MFI (g/10min.)	1	1	1	30
Crystallinity (%)	18	34	13	21
Hardness (Shore D)	22	47	11	20
Tensile Strength (MPa)	9.76	27.90	3	3
Tensile Elongation (%)	810	750	1200	1000
Octene Content (%)	38	17	45	40

2.2.2. Compounding and Specimen Production

12 different TPO formulations were generated by incorporation of PP and four chosen plastomers in different load. All the components were melt-mixed in the compounding machine (Twin Screw Extruder, Coperion ZSK 32). L/D ratio of the machine is 44 and the screw diameter is 32 mm. Barrel temperatures were set to 160-190 ºC and screw speeds were set to 65 rpm. The melt was cut into pellets at the die head by underwater pelletizing system. The formulations of TPO compounds with different loading levels of PP and plastomers (30%, 50% and 70%) were represented in Table 2.

Table 2. TPO compounds with various plastomer load

Composition	**PP**	**A**	**B**	**C**	**D**	**E**	**F**	**G**	**H**	**I**	**J**	**K**	**L**
Polypropylene	100	30	30	30	30	50	50	50	50	70	70	70	70
Engage 8100		70				50				30			
Engage 8540			70				50				30		
Engage 8842				70				50				30	
Engage 8407					70				50				30

Specimen production was done by molding of the pellets by injection molding machine (ENGEL Victory 90). Injection parameters were set as barrel temperature of 180-190 °C, injection velocity at 25 mm/s and injection pressure at 55-60 bar. Molded specimens are thin square plaques having dimensions as 130x130 mm, thick plaques having 130 mm length and 6 mm width and the dog bone tensile test samples, which were cut from the square plaques, with 115 mm length and 2 mm thickness according to ISO 37 [30].

2.2.3. Characterization Methods

Characterization part contains structural analysis of plastomers by NMR and molecular dynamic simulations and mechanical and thermal measurements for 12 TPO samples.

2.2.3.1. Nuclear Magnetic Resonance (NMR) Spectroscopy

Structural analysis of plastomers was performed by Varian Inova 500 MHz NMR Spectrometer. Homogeneous solutions of plastomer samples were obtained by dissolution of plastomers in deuterated chloroform (CDCL3) which placed in an

ultrasonic bath which was set to 40℃ and mixed with a vortex mixer. Then 1H NMR measurements of these solutions were conducted. The subunit ratios of plastomers structures were calculated by the comparison areas under the NMR peaks.

2.2.3.2. Molecular Dynamics (MD) Simulations

The molecular chain conformation of plastomers obtained from NMR were used in MD simulations which were performed by Materials Studio 6.0 package [31]. Geometrically optimized plastomer chains by Smart Algorithm were put in simulation boxes created by using Amorphous Cell (AC) Construction [32] tool. 10 chains were loaded in these cubic boxes which have length of 25.4 Å and cut-off distance of 12.5 Å having temperature at 298 K and the density as 0.86 g/cm^3. Then, Equilibrium Simulations and Production MD Simulations by these AC constructions which were run by Universal Forcefield Forcite dynamic calculation tool [33]. Simulation parameters were adjusted specifically for each simulation such as for Equilibrium Simulation, canonical ensemble (NVT) was chosen, atomic velocities were set to random and total simulation time to 150 ps. Following this, Production MD Simulations was conducted in isothermal-isobaric ensemble (NPT), velocities were set to current (last frame of NVT ensemble) and total simulation time was set to 1 ns. Both of these simulations were carried out at 1 atm pressure and temperature at 298 K using Andersen-Berendsen thermostat-barostat [34,35].

Equilibrium and Production MD simulations of PP were also conducted at the same conditions as plastomers, only changing density into 0.89 g/cm^3. Density fields, the Radii of Gyration [36] analysis realized made from Production MD simulation outputs. Additionally Flory-Huggins Parameter [37] calculation was made from the Hildebrand solubility parameters [38] obtained from Cohesive Energy Density (CED) [39] calculation tool.

The calculation of Hildebrand solubility parameter (δ) and Flory-Huggins interaction parameter (χ) were represented below [23]:

$$\delta = \sqrt{\frac{E_{coh}}{V}} = \sqrt{CED} \qquad \chi_{ij} = \frac{V_M}{K_B T} (\delta_i - \delta_j)^2$$

where Ecoh and CED represent cohesive energy and cohesive energy density, respectively for solubility parameter calculation and V_M is the molecular volume of plastomers.

MD simulations were carried out for a set of molecules that contains four plastomers used in formulations. The backbone length was kept constant at 26 carbon atoms. This set of molecules, which is represented in Table 3, were named according to octene and ethylene content where the number after "O" signifies the number of octene side chain and the number after "E" signifies the ethylene branching. Also MD simulations of plastomers with highest and lowest crystallinity in PP matrix which corresponds to TPO samples were studied. Similar nomenclature system was applied for these samples such as number after PP signifies the PP load and the number after plastomer code signifies the plastomer load. This additional nomenclature for TPO samples having highest and lowest crystallinity plastomers, different than the ones given in Table 2, was used only for the interpretation behavior of plastomers in PP matrix and aims a better understanding of structure-function relationship of these chosen samples. These samples were represented in Table 4 with both nomenclature.

Table 3. MD Simulation dataset of plastomers according octene/ethylene content

MD Dataset for plastomers	**O1E0**	**O2E0**	**O3E0**	**O5E0**	**O1E1**	**O1E2**
Octene side chain	1	2	3	5	1	1
Ethylene side chain	0	0	0	0	1	2

Table 4. MD Simulation dataset of plastomers in PP matrix according to PP and plastomers % loading

	PP-O3E0 (13% cryst.)			**PP-O1E1 (34% cryst.)**		
MD Dataset for plastomers in PP	**PP30-O3E070 (C)**	**PP50-O3E050 (G)**	**PP70-O3E030 (K)**	**PP30-O1E170 (B)**	**PP50-O1E150 (F)**	**PP70-O1E130 (J)**
Plastomer Load (%)	70	50	30	70	50	30
PP Load (%)	30	50	70	30	50	70

2.2.3.3. Mechanical Measurements

For mechanical properties of samples a universal tensile testing machine (Zwick Roell Z010) having test speed is 500 mm/min. and gage length with 25 mm, according to ISO 37, was used. Properties such as 100% modulus, 300% modulus, tensile strength at break and elongation at break were measured by using dog bone tensile test with 115 mm of length and 2 mm thickness.

2.2.3.4. Thermal Measurements

As thermal tests: melting temperature (T_m) and crystallization temperature (T_c) in ºC, enthalpy of melting (ΔH_m) and enthalpy of crystallization (ΔH_c) in J/g measurements were done by Differential Scanning Calorimetry (Mettler Toledo DSC 3). The measurements were conducted at temperatures between -80 and 200 °C at heating or cooling rate of 40 K/min. under nitrogen environment with 50 ml/min gas flow rate according to ISO 11357-3. The melting enthalpy and the crystallization enthalpy values were used to calculate the crystallinity of the plastomer and PP in the compounds by the following formulas [40];

$$X_{C,h} = \frac{\Delta H_m}{\Delta H_m^\circ} * 100 \qquad X_{C,c} = \frac{\Delta H_c}{\Delta H_c^\circ} * 100$$

where ΔH_m, ΔH^o_m, ΔH_c, ΔH^o_c are the melting enthalpy, latent heat of melting value of %100 crystalline PP, the enthalpy of crystallization and the latent heat of crystallization value of %100 crystalline PP, respectively. Latent heat of fusion and crystallization were taken as 207 J/g as indicated in literature [40]. Also, $X_{C,h}$ and $X_{C,c}$ indicate the degree of crystallinity resulting from heating and cooling cycles, respectively. The degree of crystallinity of plastomers in the compound were also calculated likewise. Before crystallinity calculation of plastomers, knowing the crystallinity percent of the analyzed plastomer, the latent heat of fusion and crystallization of 100% plastomers were calculated from DSC curves. Following the crystallinity calculations, the results of the difference between the crystallinity coming from ΔH(melting) and ΔH(crystallization) for both PP and plastomer were evaluated.

2.2.3.5. Hardness Measurements

For hardness measurements an automatic hardness tester (Gibitre Shore D Hardness Tester) was used and measurements were conducted by using the plaques with 6 mm thickness. According to ISO 7619-1, the average of the hardness values obtained from

three different points of the plaques by application of 5 kg of force for 15 seconds with the needle at the tip of the instrument were reported as the actual hardness value for TPO samples.

2.2.3.6. Mold Shrinkage Measurements

Mold shrinkage values of the samples were obtained by calculation of the ratio between the corresponding length of standard mold and the corresponding length of the square plaques for both parallel and perpendicular to flow directions by using a digital caliper (Mitutoyo NTD25-20AX). Then, mold shrinkage value was expressed in percentage.

2.3. Results and Discussion

This part of the thesis involves the results of structural analysis of plastomers and physical, mechanical, and thermal properties of the samples which contains these plastomers.

2.3.1. Structural Characterization of Plastomers

Structural analysis of plastomers involves NMR and MD simulations. With the help of NMR analyses, octene and/or ethylene content present in the structure of plastomers were calculated. Then, by looking at octene and/or ethylene content results, MD simulations of these structures were conducted in order to observe the effect of octene and ethylene content of plastomers on their crystallinity and moreover the effect of plastomer crystallinity in PP matrix. The octene content examination was done by MD simulations of plastomer molecules containing 1 to 5 octene side chains and without ethylene branching, such as O1E0, O2E0, O3E0 and O5E0. In a similar way, the effect of ethylene branching was studied by MD simulations of plastomer molecules having 1 to 2 ethylene side chains with constant octene side chains such as O1E1 and O1E2 and compared with O1E0.

2.3.1.1. NMR Analysis of Plastomers

For the calculation of octene and/or ethylene side chain content by NMR peaks, length of octene and ethylene side chains and length of backbone were estimated. The steps of calculating the octene and/or ethylene side chain content is as the following:

Step 1: Calculation of the number of octene and/or ethylene side chain by the number of hydrogens represented with the total area under the peak between 0.95 – 0.75 ppm since it signifies the hydrogens coming from CH_3 that are ending groups.

Step 2: 6 hydrogens coming from the two sides of the backbone end groups were eliminated in order to calculate side end group hydrogens.

Step 3: Then the number of hydrogens were divided by 3 since a side ending group contains 3 hydrogens (CH_3). **(*)** The decision of whether these hydrogens coming from octene or ethylene side chain was made according to further calculation such as octene content and corresponding crystallinity of plastomer. The found values were compared to the literature information.

Step 4: Length of backbone was calculated the number of carbons at the backbone from the calculation of number of hydrogens represented with the area under the peak between 1.45 – 1.10 coming from CH_2.

Step 5: The number of hydrogens at backbone was found by subtracting the number hydrogens and carbons at the side chains (total # of hydrogen – (# of hydrogen * # octene side chains)).

Step 6: The number of carbons at backbone was calculated by dividing the number of hydrogens at the backbone by 2 since every carbon at backbone contains 2 hydrogens.

Step 7: After finding the total number of carbons (a) and hydrogens (b) on one molecule by summing up the carbons and hydrogens coming from backbone, backbone end groups, side chains and junctions which is equal to the side chain number, the total molecular weight of the molecule (c) and the molecular weight of octene side chains were calculated (d). Finally the ratio between the molecular weight of octene side chains and the total molecule gave the octene content of the treated plastomer (e). This calculation is represented in Table 5 for each plastomer with the corresponding steps.

Table 5. Octene and ethylene content calculation

Calculation Steps		Engage 8842	Engage 8100	Engage 8407	Engage 8540
Octene/Ethylene Calculation	**(1)** Total # of H from CH_3	17	12	16	13
	(2) # of H from CH_3 at side chain	11	6	10	7
	(3) # of octene side chain	3	2	2	1
	(3*) # of ethylene side chain	0	0	1	1
Backbone Length Calculation	**(4)** Total # of H from CH_2	85	68	40	86
	(5) # of hydrogen at backbone	55	48	30	76
	(6) # of carbon at backbone	27	24	15	38
Octene Content Calculation	**(7a)** Total # of carbon	50	40	28	49
	(7b) Total # of hydrogen	102	82	58	100
	(7c) Total Molecular Weight	702	562	394	688
	(7d) Total octene molecular weight	336	224	112	112
	(7e) Octene Content (%)	**47.8**	**39.8**	**28.4**	**16.2**

According to the octene and ethylene side chain content analysis results of plastomers, one can observe that plastomers having same type of ethylene-1-octene chemical formula can have different number of octene side chains and different number of ethylene branching that affect their octene content. The clarification of plastomer structures are ensured by the comparison of NMR octene content calculations to the TDS octene content values, explained in Table 1, by obtaining accurate number of octene and ethylene side chains with respect to their octene contents. The possible conformations of plastomer are represented in Figure 4.

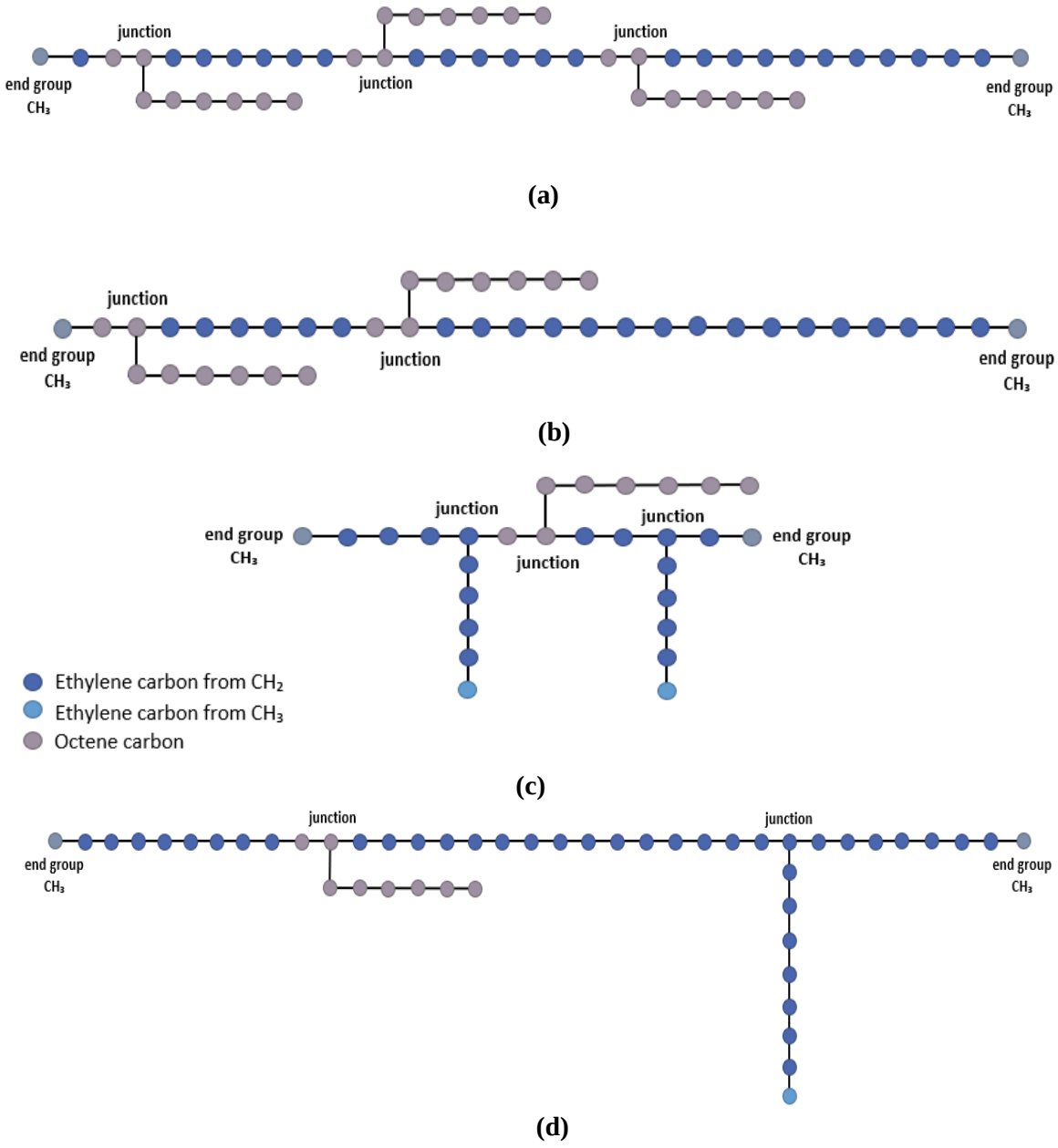

Figure 4. Schematics of estimated molecular structures of plastomers (a) ENGAGE 8842 (b) ENGAGE 8100 (c) ENGAGE 8407 (d) ENGAGE 8540

In order to avoid commercial names, depending on the octene and ethylene side chains numbers of plastomers, abbreviations such as O3E0 for ENGAGE 8842, O2E0 for ENGAGE 8100, O1E2 for ENGAGE 8407 and O1E1 for ENGAGE 8540 are assigned. These abbreviations and the relationship between the structure, MFI value, crystallinity and octene content of the plastomers are represented in Table 6. It is observed that decreasing octene content increases the crystallinity. Also, the backbone chain length explains the MFI value difference between O1E2 (Figure 2c) and other plastomers where an increase in MFI value (30 g/10min.) corresponds to shorter backbone chain of O1E2 than other plastomers which have either lower MFI value (1 g/10min.).

Table 6. Abbreviations of plastomers according to octene and ethylene content

Engage Code	Abbreviation	MFI (g/10min.)	Crystallinity (%)	Octene Content (wt%)
8842	O3E0	1	13	47.8
8100	O2E0	1	18	39.8
8407	O1E2	30	21	28.4
8540	O1E1	1	34	26.2

2.3.1.2. MD Simulations of Plastomers

Figure 5 represents the radii of gyration analysis of the plastomers which are obtained from the production MD simulations of plastomers carried out by the structures obtained from NMR analysis. According to Figure 5a, one can observe that R_g has a decreasing trend with increasing octene content in plastomers. This trend can be explained as increasing octene content causes plastomer chains to fold up, get a packed conformation and generate a cluster of molecule chains which can be seen in Figure 5c. This clustered structure prevents alignment of polymer chains and decrease the crystallinity as represented in Figure 5a. However, as seen in Figure 5b, the ethylene content addition, increases the R_g value which means that plastomer chains extend and become aligned as shown in Figure 5d. The alignment of these chains promote increase in crystallinity values since O1E1 and O1E2 have higher crystallinity values than O2E0 and O3E0 plastomers.

Also, Figure 5 shows the Flory Huggins parameters of plastomers against polypropylene which has the same chain length as plastomers. The compatibility between plastomers

and PP in the matrix is studied by Flory Huggins parameter. According to Figure 5a, an increase in the octene content decreases the Flory Huggins parameter of corresponding plastomer against PP. Since decreasing Flory Huggins parameter corresponds to increasing compatibility [41], one can deduce from Figure 5a that plastomer, which have lower crystallinity values according to Table 6, becomes more compatible with PP. However, Figure 5b shows that any increase in ethylene content cause an increase in Flory Huggins parameter which states for the decrease in the compatibility between PP and plastomers that have higher crystallinity. So, as a results of Figure 5, as the R_g value gets lower R_g and plastomer has clustered structure as shown in Figure 5a and 5c, PP and plastomer with low crystallinity become more compatible. On the other hand, as R_g value gets higher and plastomer has more extended structure with higher ethylene content, PP and the plastomer with high crystallinity become less compatible as shown in Figure 5b and 5d.

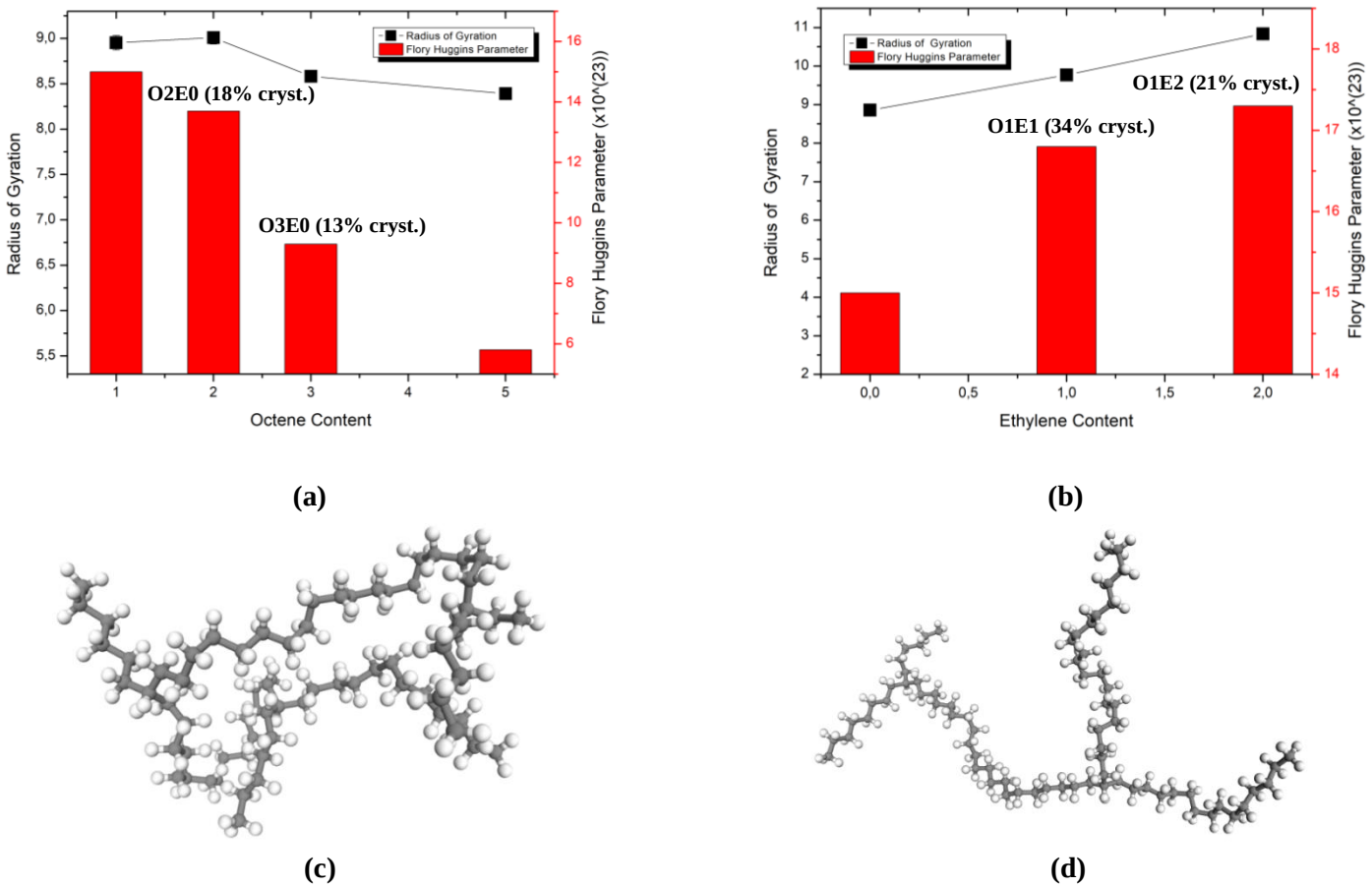

Figure 5. Radii of Gyration (R_g) and Flory Huggins Parameter values obtained from MD simulations with respect to octene (a) and ethylene (b) contents of plastomers and 3D chemical structures of plastomers selected from MD simulations represent packed O3E0 (c) and extended O1E1 (d) conformations. The chemical structures are in ball-and-stick representations where C and H atoms are represented in gray and white, respectively. Remaining plastomer molecules present in MD simulation boxes are turned off for better visualization.

Moreover, in order to examine the behavior of plastomers in PP matrix, MD simulations of plastomer + PP matrix in the compound form were carried out for compounds that contain plastomers with lowest (O3E0 with 13% cryst.) and highest crystallinity (O1E1 with 34% cryst.). The Rg values of PP and plastomer in these compound were analyzed and their density fields with increasing plastomer content in the compound were studied. According to Figure 6a and 6b, the R_g of plastomer is higher than the R_g of PP for both of the compounds containing high and low crystalline plastomers. This behavior results from the R_g values of plastomers in neat form (Fig. 5a, Fig. 5b) due to their octene and ethylene contents. That is to say, as represented in Figure 6a, R_g value of PP decreases and its structure gets more clustered as the R_g value of low crystalline plastomer increases with increasing plastomer load. The density fields of MD simulations with low crystalline plastomer at low loading level supports this behavior since there is a formation of an interpenetrating structure as shown in Figure 6c. However, higher load of the same plastomer in PP matrix causes PP chains to become more packed and forms clusters in plastomer network. So, these clusters are unable align and get crystallize. On the contrary, as shown in Figure 6b, the difference between R_g values of plastomer and PP decreases with increasing plastomer load of high crystallinity. As shown in Figure 6d, as the R_g values of PP and plastomer get close, the structure becomes more interpenetrated with increasing plastomer load. Also, increasing plastomer load encourage both PP and plastomer to become more aligned and show phase separation at highest plastomer load.

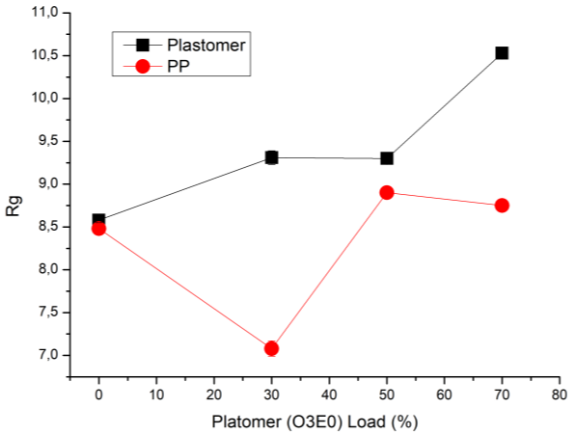

(a)

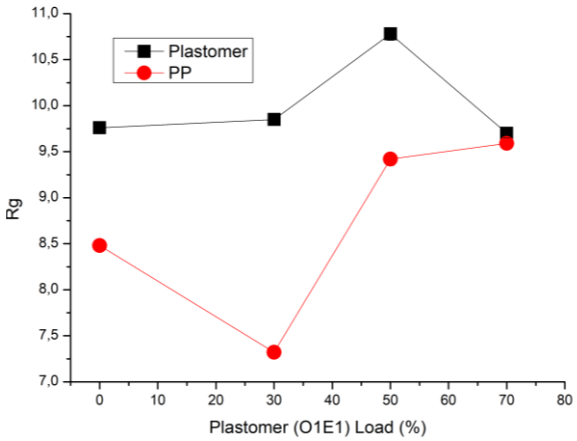

(b)

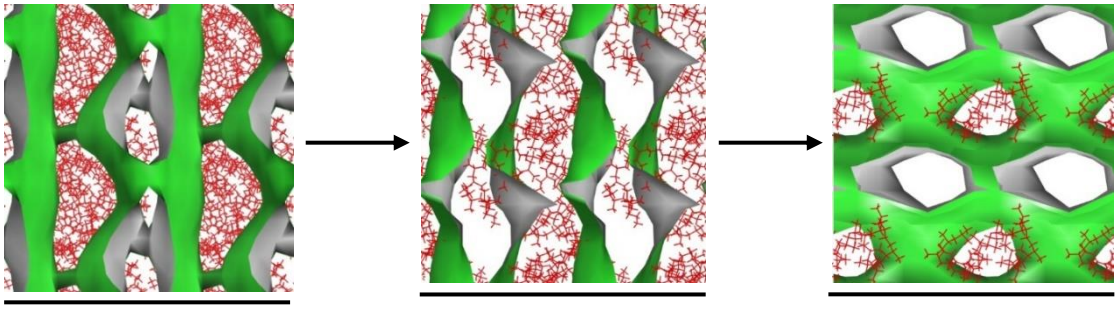

5 nm PP70-O3E0**30**

5 nm PP50-O3E0**50**

5nm PP30-O3E0**70**

(c)

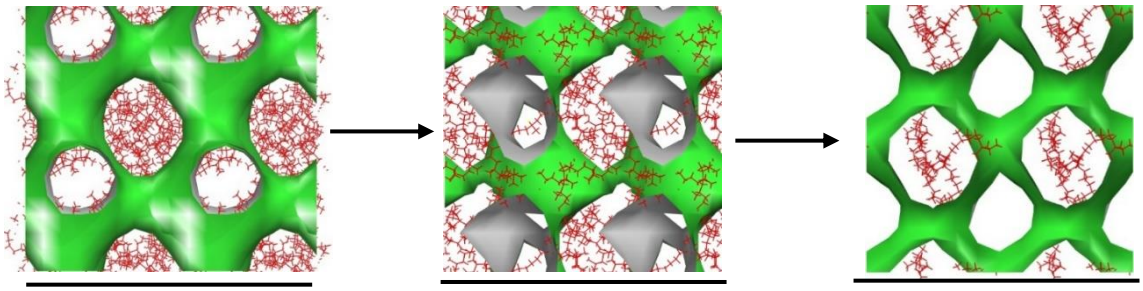

5 nm PP70-O1E1**30**

5 nm PP50-O1E1**50**

5 nm PP30-O1E1**70**

(d)

Figure 6. Effect of plastomer load on radii of gyration obtained from MD simulations (a) with plastomer having lowest crystallinity (O3E0), and (b) with plastomer having highest crystallinity (O1E1) and representation of density fields of MD simulations of plastomers (green) + PP (red, in stick representation) matrix with increasing plastomer load for (c) lowest crystalline plastomer (O3E0), (d) highest crystalline plastomer (O1E1). 3D molecular structures of plastomers were turned off for better visualization.

2.3.2. Physical and Mechanical Characterization of TPO Compounds

Physical and mechanical characterization of the TPO samples from A to L that contains the investigated plastomers at 30%, 50% and 70% loading levels were investigated. The effect of the crystallinity and MFI value of plastomers depending on their different chemical structures, on physical and mechanical properties were examined.

2.3.2.1. Physical Characterization

Physical characterization contains the mold shrinkage results of TPO compounds. Figure 7 represents the effects of plastomer loading on mold shrinkage values. Figure 7a to Figure 7c show effect of plastomer with constant low MFI value (1 g/10min.) but different crystallinity on mold shrinkage whereas Figure 7d shows effect of plastomer having high MFI (30 g/10min.) value and medium crystallinity.

As shown in Figure 7a, the anisotropy and mold shrinkage values decrease with the incorporation of plastomer having high crystallinity value (34%) at low loading level when compared to other loading levels but increase with the increasing loading level. However, as seen in Figure 7b and Figure 7c, mold shrinkage values and anisotropy decrease with increasing loading level when plastomers with medium and low crystallinity values (18% and 13%) are incorporated. Even, at the highest loading level (70%), the anisotropy disappears and the minimum mold shrinkage values are obtained especially in the case of O3E0 incorporation. So, since similar results are reported by Warner et al. [9], one can conclude that the anisotropy and the mold shrinkage values in both parallel and perpendicular directions decrease as the crystalline phase decreases and amorphous phase increases in the material. This behavior can be explained in such a way that when the crystallinity of the material increases the mold shrinkage values also increases because during the cooling down process of polymer having high crystallinity, crystals form and shrink much more than the amorphous regions. The difference between the shrinkage rates of crystalline and amorphous phases causes an imbalance in the material and a net increase in shrinkage [42,43]. In the meantime, this behavior is supported by MD simulation results since plastomers with low crystallinity, increases its own R_g but decreases the R_g of PP in the compound with increasing plastomer load. So, PP become more packed and forms clusters which are unable to be aligned and get crystalline. So, the mold shrinkage value decreases with the use of low crystalline plastomers.

Two of the plastomers having medium crystallinity (O2E0 (18%) and O1E2 (21%)) with one of them having low (1 g/10min.) and one of them having high (30 g/10min.) MFI value, respectively are chosen to observe the effect of MFI value of plastomer on mold shrinkage. Figure 7b and 7d represent the mold shrinkage values in perpendicular and parallel directions of compounds containing O2E0 and O1E2 respectively, with different loading levels. When these two graphs are compared the minimum mold shrinkage values in both directions and the minimum anisotropy is found in Figure 7d, with the addition of plastomer having high MFI and medium crystallinity value at 50% loading level. So, the optimum loading level can be considered as 50% because the mold shrinkage values at parallel direction and the anisotropy increases at low and high loading levels of plastomer O1E2. This mold shrinkage behavior difference of plastomers O2E0 and O1E2 stems from the relation of MFI with molecular weight of the material. Despite to similar crystallinity values, lower mold shrinkage values of the plastomer with higher MFI value can be explained in such a way: high MFI value corresponds low molecular weight or shorter polymer chain. Figure 4c shows that plastomer named O1E2, with high MFI value, has a shorter chain structure than other plastomers having longer chains and low MFI value. Also, as represented in Figure 5, O1E2 has higher R_g than O2E0 which shows that the chains of O1E2 are in a shorter but more extended state whereas the chains of O2E0 are longer and more packed with lower R_g. Since shorter and extended chains are more prone to disrupt PP matrix, they can prevent the formation of the crystalline structure of PP and mold shrinkage [32]. The difference of mold shrinkage between loading levels of O1E2 can be explained by the behavior difference of the chains of plastomer in PP matrix depending on the loading level. The reason of anisotropy at low loading level may come from the lack of enough plastomer content in matrix which leads to insufficient disruption of crystalline phase of PP. This results in insufficient decrease of the mold shrinkage in parallel direction. However, despite to its high MFI value, same plastomer has high mold shrinkage values at high loading level which may result from the formation of crystalline phase by plastomer itself due to higher R_g value and extended chain structure as represented in Figure 5b and 5d. These characteristics show that, despite to its higher crystallinity than O2E0, O1E2 has its lowest mold shrinkage values and isotropy at 50% loading level due to its short molecular chain and high MFI value.

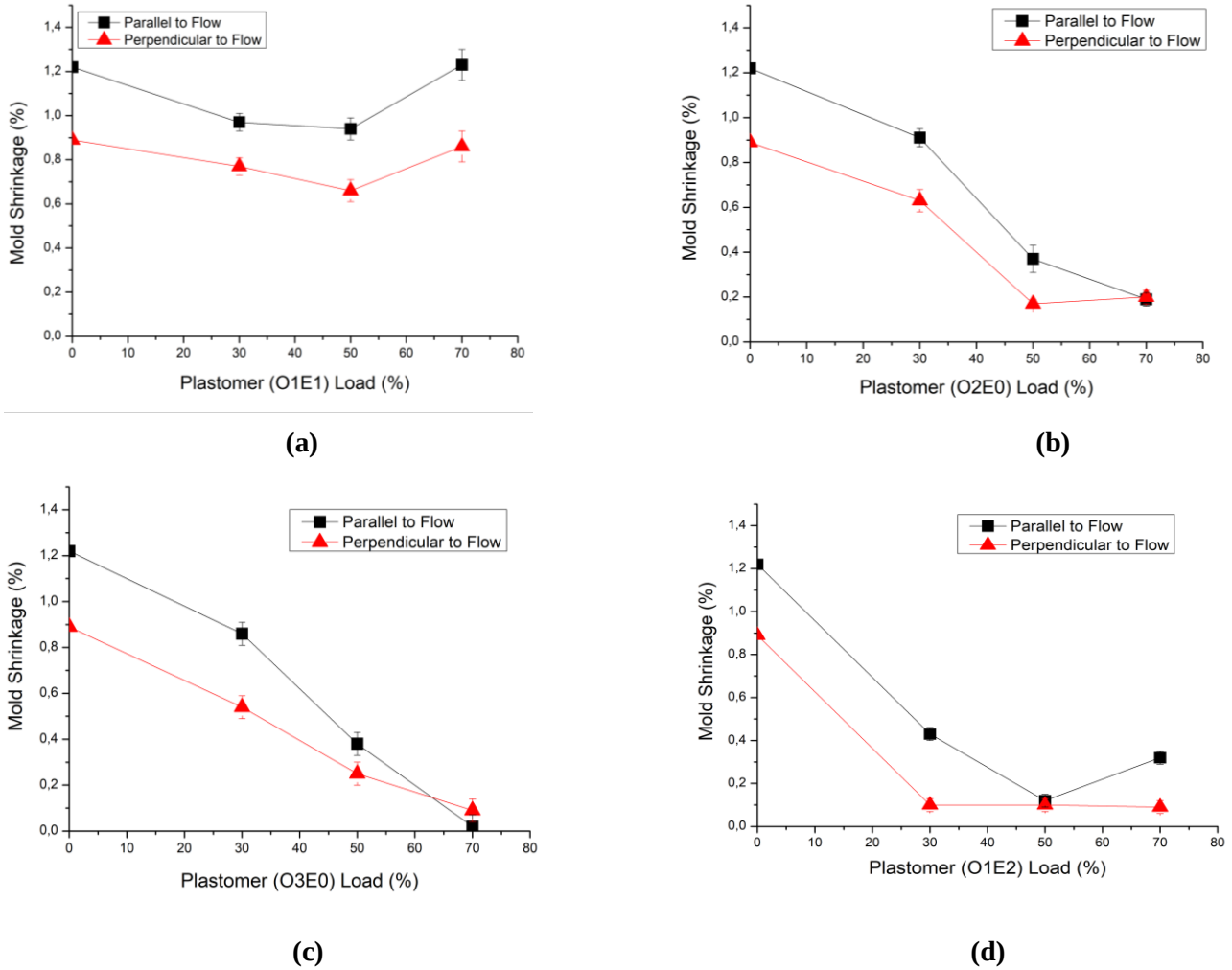

Figure 7. Plastomer load vs. mold shrinkage of samples (a) O1E1 (34% crystallinity and 1 g/10min. MFI) (b) O2E0 (18% crystallinity and 1 g/10min. MFI) (c) O3E0 (13% crystallinity and 1 g/10min. MFI) (d) O1E2 (21% crystallinity and 30 g/10min. MFI)

2.3.2.2. Mechanical Characterization

Figure 8 represents the results of mechanical characterization such as tensile strength, 100% and 300% modulus, elongation at break, tear strength and hardness of TPO compounds at different plastomer loading levels (30%, 50% and 70%) with plastomers having different crystallinity and MFI value.

Figure 8a shows that at low plastomer loading, tensile strength values of compounds with each plastomer decreases but after 50% and higher plastomer loading levels the tensile strength values depend on the crystallinity of the incorporated plastomer. The highest tensile strength value is obtained with the compound containing the plastomer with highest crystallinity (O1E1) at 70% loading whereas other compounds with rest of the plastomers having lower crystallinity show lower tensile strength values. This behavior can be explained in such a way that when the crystallinity of the plastomer decreases, it affects the strength of intermolecular bonding ensured by crystalline phase. So, the total strength of the polymer decreases compared to more crystalline structures as indicated by Balani et al. [44]. Besides, at 70% loading level, the lowest tensile strength is obtained by O1E2 which has the highest MFI value. Since it has shorter and more extended chains, it disrupts the crystallinity of the polymer matrix more than other plastomers [45].

Figure 8b and 8c represent the 100% and 300% modulus values of TPO compounds respectively, where one can observe a decreasing behavior as the plastomer load in compounds increases which does not depend on the crystallinity value of plastomers. However, the moduli values of compounds for each plastomer depend on crystallinity of plastomers since both moduli values of compounds containing highest crystallinity show the highest values at high loading amounts (50% and 70%) and the compounds containing lowest crystallinity (O3E0) shows the lowest moduli values. This behavior strongly supports the theory of increasing crystalline phase increases mechanical properties [32].

Figure 8d represents the elongation at break values of TPO compounds which have an increasing trend with increasing plastomer load. Compounds with plastomers named O3E0 and O2E0 which have low crystallinity values such as 13% and 18% respectively, show higher elongation values while compounds with plastomers named O1E2 and O1E1 which have relatively higher crystallinity values such as 21% and 34% respectively, show lower elongation values. This difference stem from the side chain variety between the plastomers. O3E0 and O2E0 have higher elongation values because low crystalline

structures contain only octene side chains having low Rg and less ordered structure with more free molecular chains which enable them to elongate. On the other hand, O1E2 and O1E1 show lower elongation values because they have higher crystalline structure with more extended ethylene branching and ordered molecular chains that restrict the mobility and elongation. However, O1E2 and O1E1 containing longer ethylene side chains which are more extended and ordered molecular chains have restricted mobility and elongation [46,47].

Figure 8e shows that tear strength also have a dependence on crystallinity of the incorporated plastomer. Compounds containing high and medium crystallinity plastomers, which are O1E1 and O2E0, at 50% loading level show highest tear strength values whereas the plastomers with high MFI value, O1E2, and low crystallinity, O3E0, show the lowest tear strength. The high chain orientation resulting from more extended chain structure may explain the increase in resistance to tear and decrease of tear propagation behavior of compounds with high and medium crystalline plastomers [48]. Additionally, the lowest tear strength values for every kind of plastomer are obtained at highest plastomer load because highest plastomer load means less crystalline phase in the compound.

Figure 8f shows that increasing plastomer content decreases the hardness values because since all plastomers have lower hardness values than the hardness of PP, any decrease in the crystalline phase of PP by plastomer addition, decreases the overall hardness values of TPO compounds. The crystallinity and hardness values of neat plastomers may explain the different hardness values of TPO compounds at the same load level. Compounds with high crystallinity plastomers results in higher hardness values because the high crystallinity and hardness value of neat plastomer increases the overall hardness of the TPO compounds [44,49]. For example, O1E1 which has the highest crystallinity (34%) and correspondingly the highest hardness value (47) in neat form, shows the highest hardness values when loaded into TPO compound at every loading level. However, O3E0 which has the lowest crystallinity (13%) and the lowest hardness value (11) and gives the lowest hardness value in TPO compound.

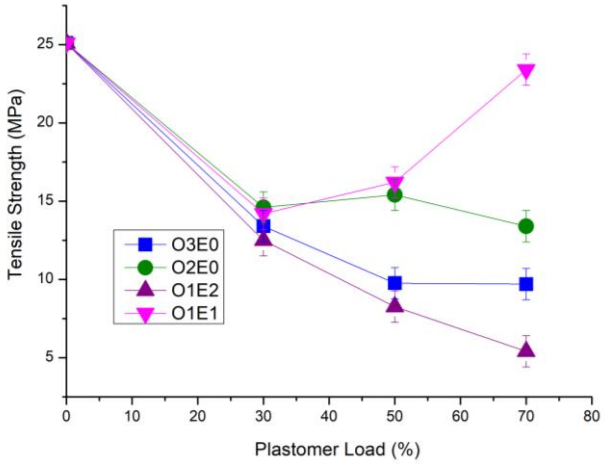
Tensile Strength (MPa)
Plastomer Load (%)
O3E0
O2E0
O1E2
O1E1

(a)

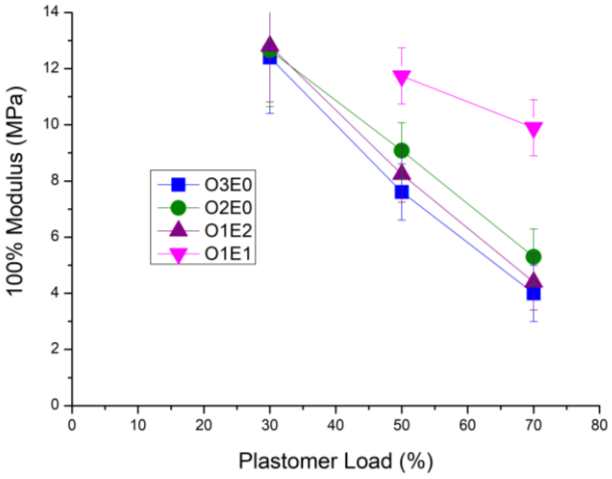
100% Modulus (MPa)
Plastomer Load (%)
O3E0
O2E0
O1E2
O1E1

(b)

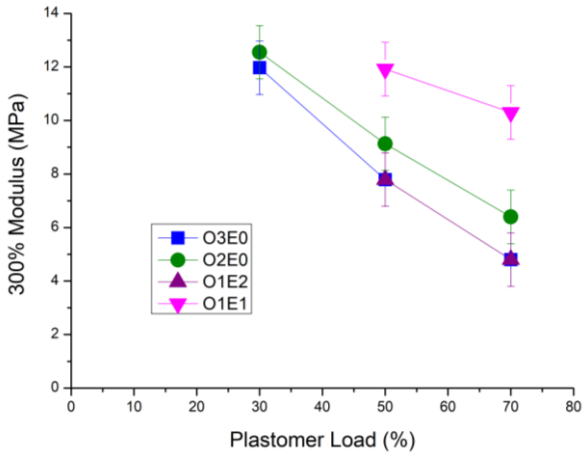
300% Modulus (MPa)
Plastomer Load (%)
O3E0
O2E0
O1E2
O1E1

(c)

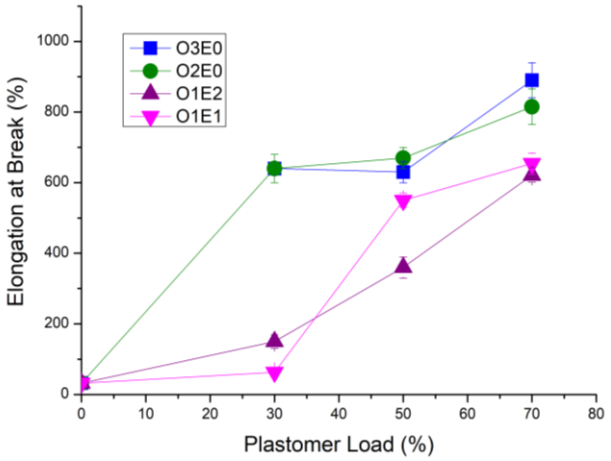

(d)

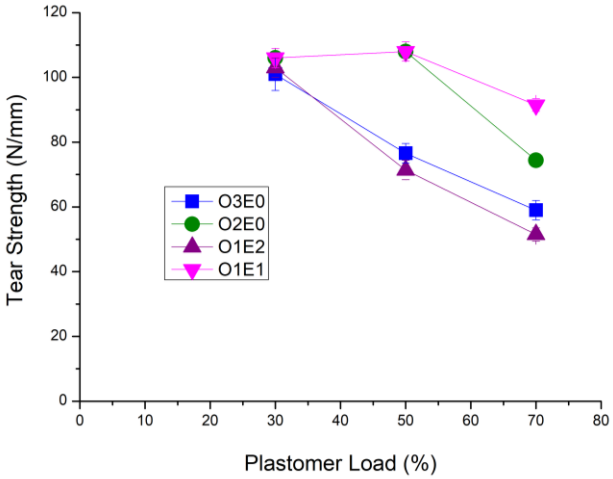

(e)

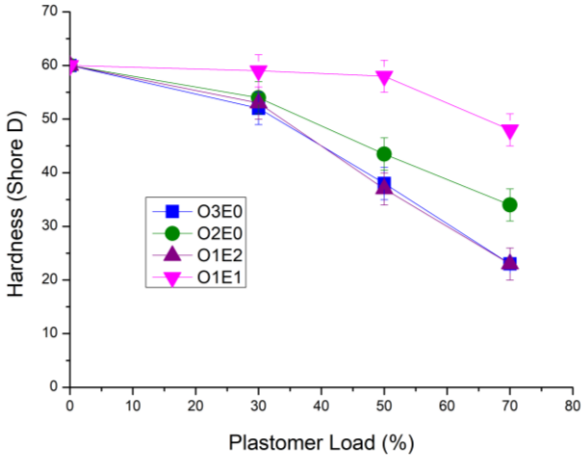

(f)

Figure 8. Effect of plastomer load on (a) tensile strength (b) 100% modulus (c) 300% modulus (d) elongation at break (e) tear strength (f) hardness

2.3.3. Thermal Characterization

Table 7 represents the melting and crystallization temperatures of PP and plastomer in the compounds and the degree of crystallinity of PP and plastomer in the compound resulting from heating and cooling cycles. The total crystallinity of the individual compound corresponding to either heating or cooling stage can be considered as the sum of crystallinity of plastomer and PP in corresponding cycle.

Table 7. Thermal property results of TPO compounds

	Thermal Properties				
Samples	**Components; Plastomer vs. PP**	**Melting Temperature (Tm) (°C)**	**Heating Crystallinity ($X_{C,h}$) (%)**	**Crystallization Temperature (T_C) (°C)**	**Cooling Crystallinity ($X_{C,c}$) (%)**
PP	-	-	-	-	-
	PP (100%)	163.25	34.09	110.60	38.63
A	O2E0 (70%)	63.60	10.82	45.94	14.35
	PP (30%)	165.68	30.11	96.13	29.14
B	O1E1 (70%)	110.40	34.10	72.50	2.46
	PP (30%)	165.29	36.47	93.94	71.26
C	O3E0 (70%)	-	-	-	-
	PP (30%)	165.32	40.51	11.85	40.09
D	O1E2 (70%)	65.75	10.11	49.27	3.33
	PP (30%)	163.65	36.42	110.66	39.14
E	O2E0 (50%)	-	-	-	-
	PP (50%)	164.26	33.41	118.26	35.85
F	O1E1 (50%)	110.66	31.41	95.09	26.27
	PP (50%)	146.43	35.82	116.05	36.66
G	O3E0 (50%)	-	-	-	-
	PP (50%)	165.25	38.25	118.58	36.96
H	O1E2 (50%)	-	-	-	
	PP (50%)	164.29	38.35	119.19	40.77
I	O2E0 (30%)	63.77	4.23	73.42	1.28
	PP (70%)	164.22	38.50	120.33	40.79
J	O1E1 (30%)	110.02	30.60	95.38	24.92
	PP (70%)	164.84	39.14	117.86	41.26
K	O3E0 (30%)	-	-	-	
	PP (70%)	164.18	39.63	119.55	41.72
L	O1E2 (30%)	-	-	-	-
	PP (70%)	163.15	44.50	119.12	44.09

Samples from A to D have high plastomer loading (70%) with different crystallinity values. Among them, only sample C, containing the lowest crystalline plastomer (O3E0) has a single peak corresponding to PP whereas sample A,B and D have double peaks

coming from plastomer and PP. Comparing the degree of crystallinities, coming from melting and crystallization processes, of PP of these compounds, the highest difference is seen in sample B where the degree of crystallinity of PP changes from 36.47% to 71.26% due to incorporation of plastomer having highest crystallinity while the degree of crystallinity of the incorporated plastomer decreases from 34.10% to 2.46%. This increase in the degree of crystallinity of PP supports that incorporation of plastomer with highest crystallinity increases the degree of crystallinity of PP in compound B and results in the highest mold shrinkage values as 1.23% and 0.86% in parallel and perpendicular to flow direction, respectively. However, the sample C, containing the lowest crystalline plastomer (O3E0), show only one melting and crystallization peak corresponding to PP which means that plastomer does not form extra crystalline regions and does not contribute to total crystallinity of the compound so, result in a compound with the lowest total crystallinity value. Also, since there is no contribution of the plastomer on PP crystallization, a significant difference between the degree of crystallization of PP is not observed.

Samples from E to H have medium plastomer loading (50%) with different crystallinity values. The effect of decreasing plastomer load can be observed by the disappearing plastomer peaks in E, G and H compounds which have low and medium crystalline plastomers. However, the effect of plastomer having highest crystallinity is still obvious in the compound F which has double melting and crystallization peaks. Although, there is not a significant difference between the degree of crystallinity coming from melting and crystallization processes, due to the double peak, the highest total crystallinity and the high mold shrinkage values (0.96% and 0.66%) are observed in the compound F which has the highest crystalline plastomer (O1E1).

Finally, the samples from I to L have lowest plastomer loading (30%) with different crystallinity values. The effect of the highest crystalline plastomer is also obvious in compound J having highest total crystallinity value both at melting and crystallization processes even with 30% plastomer loading. High mold shrinkage values of compound J also support the effect of highest total crystallinity with values such as 0.97% and 0.77% in parallel and perpendicular to flow direction, respectively. However, the other compounds with 30% plastomer loading, plastomer have no contribution for total crystallinity (compound K and L) or have so little contribution (compound I).

2.4. Conclusion

This study was performed to fully understand the effect of microstructure of plastomers on physical and mechanical properties of TPO materials that these plastomers are incorporated. NMR and MD simulation results showed that the molecular structure, octene/ethylene side chain content, and molecular conformations of plastomers govern their microstructure and the crystallinity. They change the physical and mechanical traits of final TPO products in which these plastomers are incorporated. The increasing octene content in plastomers decreases R_g values of plastomers resulting in a more clustered state while an increase in ethylene content in plastomers increases the R_g, which results in more extended structures. The packed conformations evident from low R_g results in a decreased the crystallinity of plastomer since clustered states corresponds to more amorphous structures. In addition, enhanced compatibility with decreasing Flory Huggins parameter is observed between plastomers and PP chains at low crystalline plastomers having only 1 octene side chain. On the contrary, extended conformations (with higher R_g) increases the crystallinity of plastomer as extended forms of polymeric chains are more capable to align regularly and become crystalline. In these plastomer-PP couples, a decrease in compatibility between PP and highly crystalline plastomers which have ethylene branching along with octene side chains. Therefore, increasing octene side chain content in the plastomer structure causes decrease in R_g of chains and crystallinity value of plastomer forms amorphous interpenetrated structures which decreases the mold shrinkage of the final TPO product. On the other hand, ethylene content in the structure increases the R_g of chains and crystallinity value of plastomer forming more extended crystalline structures by phase separation. This kind of structure causes increase in the mold shrinkage value of final TPO products.

The best results in terms of low mold shrinkage values in parallel and perpendicular to flow direction are obtained by TPO compound containing 70% plastomer O3E0 (13% crystallinity and 1g/10 min.) and 30% copolymer PP (sample C). However, that TPO compound yield lower tensile strength and tear strength while it has higher elongation at break value. TPO compound containing 70% plastomer O2E0 (18% crystallinity and 1g/10 min.) and 30% copolymer PP (sample A) is the optimum material with isotropic low mold shrinkage values in parallel and perpendicular flow direction and high mechanical properties (tensile strength, elongation at break and tear strength).

CHAPTER 3

3. Non-Solar Light Absorptive Filler Incorporation into Thermoplastic Polyolefins to Create Black Cool Surface

3.1. Introduction

Energy consumption is one of the most important considerations in the world. A significant part of this consumption comes from the use of air conditioning in buildings and automotive all around the world [50]. Especially in hot summer days, the heat that is accumulated in buildings and interior of the cars due to solar radiation encourages the use of air conditioning. The excessive use of air conditioning results in high electricity consumption in buildings and high carbon emission due to higher fuel consumption for air conditioning in automotive both cause environmental damage [51,52].

Solar light that reaches to the earth, consists of wide range of wavelengths such as ultraviolet (UV) region (300-400 nm) which is invisible to eye and accounts for the 5% of the solar energy, visible (VIS) region (400-700 nm) which is the electromagnetic region that is visible to eye and consist of the colors of the rainbow. It constitutes 43% of the sunlight. Finally, the near infrared (NIR) region (700-2500 nm) which is the 52% of the solar light and having longer wavelength than visible range, they are invisible to human eye. The most important property of NIR light is that it contains the range which causes the heat production [53,54,55]. Once the light in the range of NIR is absorbed, it is converted into heat and increase the temperature of the object and its environment which promotes the use of air conditioning. However, the reflectance (R) or transmittance (T) of the sunlight as the opposite of absorptance (A) (A=1-R-T) prevents the heating up of the surface of the object that the light interacts and provides a cool surface [53,55].

The need of cool surface in automotive industry arises from the increased temperature inside the cars due to use of conventional fillers such as carbon black in the inner parts. Even though carbon black, as filler, provides good mechanical properties such as tensile strength and hardness in automotive inner parts, its high sunlight absorption property causes high heat accumulation inside the cars [56,57]. In order to compete with high heat absorption of carbon black another filler, titanium dioxide, with high solar reflectance is

used in roofing constructions but cannot be used in automotive inner parts due to its distracting property with high solar reflection [58]. So, a possible solution, especially for automotive industry, can be the use of cool black pigments which are colorant additives that maintain its black color by absorbing solar radiation at UV range but the keeps the surface cool by reflecting or transmitting the light at NIR range [59].

According to the behavior of light, these pigments can be classified as NIR reflective pigment or NIR transmitting pigments. These pigments can also be classified according to their content as organic or inorganic pigments. NIR reflective inorganic pigments mainly contain metal oxides such as chromium oxide (Cr_2O_3) or (Fe_2O_3) and can be doped with other metals in order to enhance the reflectance [59]. Sangeetha et al. investigates the effect of Cr_2O_3 nanoparticles and doped Cr_2O_3 nanoparticles with rare earth metals such as lanthanum (La) and praseodymium (Pr) on NIR reflectance due to which improved NIR reflectance results are obtained [60]. Other than chromium, copper and its oxides are also significant metal oxides that can reflect NIR radiation. The effect of pigments containing CuO submicron particles and the effect of their particle size on NIR reflectance are investigated by Gonome et al. and found that the particle size control has an effect on NIR reflectance [61]. In contrast to inorganic content, examples of pigments with organic content are very rare such as black pigment containing copper phthalocyanine, azo pigments and some perylene-based pigments. Kaur et al. study the NIR reflectance of perylene based pigments with different functionals groups at the end of perylene structures [62].

Reflection behavior of light from a material is related with its morphology such as particle size, grain size and grain boundary size or thickness. In powder samples, the reflection of light occurs from the grain boundaries which is called Diffusion Reflection and it strongly depends on the particle size. Any decrease in particle size, increases the number of grains and grain boundaries in the same volume and increases the reflection path of light in the material so the net effect of light reflectance increases with decrease in particle size and increase [52,60,63]. Liang et al. investigates the reflectance behavior of pigments containing Cr_2O_3 and effect of particle size of Cr_2O_3 particles on light reflectance and proves that decrease in particle size increases the number of grains in the same volume and thus increases the reflection path of light in pigments [64]. A similar study of Han et al. studied the iron doped $YMnO_3$ compounds as cool pigments by incorporating different amounts of iron content ($YFe_xMn_{1-x}O_3$ where x = 0, 0.05, 0.10, 0.15 and 0.20) and showed

that increasing grain size with doping results in higher light reflection since increasing grain size decreases amount light absorption and increase the reflection [65].

These pigments can be incorporated into polymers and other type of materials and can found many application areas especially in roofing of buildings or polymer materials used in automotive industry [66,67]. For instance, Raj et al. studies pigments based on terbium-doped yttrium with high NIR reflectance in polymer matrix (poly methyl methacrylate), cement slab, asbestos sheet and ceramic glazes for cool roof and surface coating applications [68]. Another study conducted by Mao et al. investigates the cooling property of $SrTiO_3$ as a new solar reflective pigment in PMMA-ceramic composites which can be applied in the electronics industry and photocatalytic fields [69]. Also, Arunima et al. develop pigments containing $WO_3/BiVO_4$ composite with enhanced NIR reflectance which has a potential to be used as cool coating at roofing and automotive body parts for saving energy [70].

This paper intends to formulate TPO compounds with cool surface despite to their black color due to the incorporation of cool black pigments. The surface temperatures and NIR reflectance values of these TPO compounds are compared to the TPO samples containing conventional pigments such as titanium dioxide and carbon black. Since these TPO compounds with black color and high NIR reflectance intended to be used in automotive parts such as bumpers and interior trims, their mechanical properties and mold shrinkage values are also investigated in order to obtain an optimum solution.

3.2. Experimental Process

3.2.1. Materials

Copolymer polypropylene named ISPLEN™ PB 180 G2M, having 20 g/10min. MFI, 25 MPa tensile strength and 60 Shore D hardness values, was supplied from Repsol Company.

Homopolymer polypropylene, named Moplen HP401R, 25 g/10min. MFI, 32 MPa tensile strength was supplied from LyondellBasell Plastic and Chemical Company. It was used in grinded form.

Plastomer named ENGAGE® 8842, having ethylene-1-octene chemical formula with 45% octene content and low (13%) crystallinity, was supplied by Dow Chemicals Company.

Two type of black cool pigments named Sicopal Black K0095 having inorganic content and known as NIR reflective pigment and Lumogen Black K0087 having organic content luminescent property and known as NIR transparent pigment were chosen from Black Cool Pigment series supplied by BASF Chemical Company. They were used in the form of masterbatch with polypropylene based resin.

BLACK SY-9240 PP, carbon black masterbatch (CB-MB) with 40% carbon black content in the polypropylene resin, from SSN-BLACK® series was supplied from Sisan Masterbatches Plastic Company.

Titanium dioxide pigment, named BLR-895, having 93% TiO2 content from Billions series was supplied from Sayman Chemical Company.

Additives such as Crodamide™ VRX (Bead) and Crodamide ER (Bead), which were supplied from Croda Chemical Company, were used as slip agents TPO compounds. Also, zinc stearate ZN-55 was supplied from Tepe Kimya Company.

3.2.2. Compounding and Specimen Preparation

Compounding process is composed of masterbatch preparation from pigments and polypropylene and the preparation of thermoplastic olefins (TPO) by incorporation of these masterbatches.

3.2.2.1. Masterbatch (MB) Compounding

Masterbatches (MB) of reflective and transparent pigments were prepared in twin screw extruder with 13% and 11% loading levels of pigments, respectively. A fair amount of wax and stearate were added into masterbatches in order to ease compounding process. Compounding was carried out by Tosaf Plastic Fabrication Company and further process condition information was not shared by the company due to confidentiality issues.

3.2.2.2. Thermoplastic Olefins Compounding

Mixtures of masterbatches with black cool pigments and other components were prepared according to pigment and copolymer polypropylene (PPC) resin content in the masterbatches. Mixture preparation of black cool pigment with TPOs and their control groups are represented in Table 8 and Table 9, respectively. The samples having “REF”, “TRANS”, “MIX” and “CB” in their nomenclature are black samples whereas samples having “Ti” are white and “empty” is colorless. The sample “empty” was prepared by taking “sample C” of the first chapter as reference which contains 30% PPC and 70% plastomer. For this part of the thesis, this sample was reproduced by adding wax and stearate in order to provide same conditions as black samples which contain wax and stearate in their masterbatches and to make more accurate comparison by only observing the effect of pigment addition. Also, the PPH grinded (powder) was only added into Ti_1 and Ti_2 in order to ease the compounding since the amount of TiO_2 in these compound are very low. In both tables, the overall filler load was represented in blue and the exact composition depending on the filler and PP amounts in the masterbatches is represented in black.

These mixtures were melt-mixed in the compounding machine (Twin Screw Extruder, Coperion ZSK 32). The barrel temperatures are set to 160-200 °C from entrance to die and screw speeds were set to 65 rpm. The mixed melt was cut into granules at die head by underwater pelletizing system.

Table 8. TPO formulations with black cool pigments at different loads

SAMPLES	FILLER LOAD (%)		COMPOSITION			
	Reflective Pigment	Transparent Pigment	PPC	Plastomer O3E0	Reflective MB	Transparent MB
REF_1	1		22.31	70	7.69	
REF_2	2		14.62	70	15.38	
REF_3	3.70		1.54	70	28.46	
TRANS_1		0.10	29.10	70		0.90
TRANS_2		0.20	28.20	70		1.80
TRANS_3		0.40	26.40	70		3.60
MIX_1	2	0.10	13.72	70	15.38	0.90
MIX_2	1	0.20	20.51	70	7.69	1.80
MIX_3	2	0.20	12.82	70	15.38	1.80
MIX_4	3.67	0.20	0	70	28.20	1.80
MIX_5	2	0.40	11.92	70	15.38	2.70

Table 9. TPO formulations with carbon black and TiO_2 at different loads as control groups for compounds with black cool pigments

SAMPLES	FILLER LOAD (%)		COMPOSITION						
	Carbon Black (CB)	Titanium Dioxide (TiO_2)	PPC	PPH grinded	Plastomer O3E0	Wax	Zinc Stearate	Carbon Black MB	TiO2 Pigment
EMPTY			29.10		70	0.40	0.50		
CB_1	1		27.50		70			2.50	
CB_2	2		25		70			5	
CB_3	4		20		70			10	
Ti_1		1	27	2	70				1
Ti_2		2	27	1	70				2
Ti_3		4	26		70				4

3.2.2.3. Specimen Preparation

Specimen preparation was carried out by molding of granules by injection molding machine (ENGEL Victory 90) with barrel temperature of 180-190 °C, injection velocity at 25 mm/s and injection pressure at 55-60 bar. Granules were molded in the shape of square plaques which have dimensions as 130x130 mm, and the thick plaques which have 130 mm length and 6 mm width. Dog bone tensile test samples were cut from the square plaques, with 115 mm length and 2 mm thickness according to ISO 37 [30].

3.2.3. Testing Methods

The testing part involves structural analysis of black cool pigments by particle size analyzer and XRF and structural analysis of TPO compounds with these pigments by SEM besides their mechanical and thermal measurements. As mechanical tests: tensile strength at break and elongation at break were conducted. Mold shrinkage values were measured as physical property and DSC results were examined as thermal characterization. Moreover, surface temperature analysis of TPOs was carried out and their surface reflectance was measured by UV-vis-NIR Spectrophotometer.

3.2.3.1. Particle Size Analysis

Particle size analysis of pigments were conducted by a laser diffraction system named Mastersizer 3000 (Malvern Instruments) in a dispersant media of water. The results were analyzed by a software v3.40: PSS0223-18 and represented as volume density percentage for each size classes.

3.2.3.2. X-Ray Fluorescence (XRF)

Metal and metal oxide content in the pigments were analyzed by X-Ray Fluorescence (XRF) spectroscopy (X-MET8000 Optimum, Oxford Instrumentation) and monitored by the software named X-MET8000 WinGUI in ppm.

3.2.3.3. Fourier-Transform Infrared Spectroscopy (FTIR) Analysis

Structural analysis of the organic pigment was performed by Perkin Elmer UATR Two FTIR Spectroscopy. The FTIR peaks obtained from the analysis were studied in order to define the organic structure of the sample.

3.2.3.4. Mechanical Measurements

Mechanical measurements were done by a universal tensile testing machine (Zwick Roell Z010) where test speed is 500 mm/min. and gage length with 25 mm according to ISO 37. Properties of TPO samples such as tensile strength at break and elongation at break were measured by using dog bone tensile test specimens having 115 mm of length and 2 mm thickness.

3.2.3.5. Mold Shrinkage Measurements

Mold shrinkage measurements were done with square plaques by using a digital caliper (Mitutoyo NTD25-20AX). Measurements were done from both parallel and perpendicular to flow directions by an internal method. The ratio between the difference of the corresponding length of standard mold and the corresponding length of the specimen was calculated and expressed in percentage.

3.2.3.6. Surface Temperature Analysis

Surface temperature analysis of the TPO compounds were conducted in a light cabin under NIR lamp having 150-watt power and being 30 cm distant from the samples as represented in Figure 9. Samples were left under NIR lamp and their surface temperatures were measured by a thermal camera (FLIR-E6390) at particular intervals of time such as initial temperature and 15, 30, 60, 120 and 180 minutes after the beginning of the analysis. The surface temperatures were recorded and the change in the surface temperatures were compared.

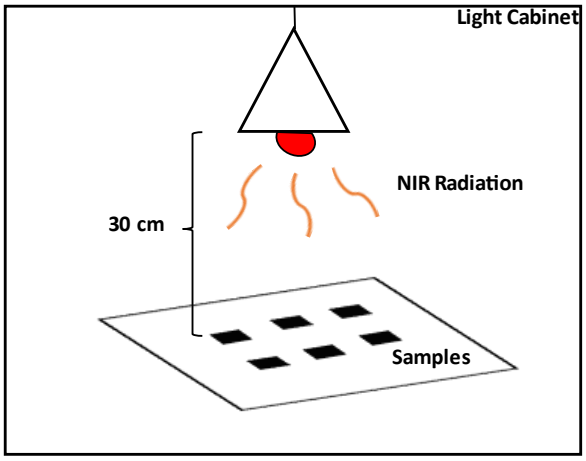

Figure 9. Representative schema of surface temperature analysis of samples

3.2.3.7. Scanning Electron Microscopy (SEM) Analysis

Structural analysis of TPOs containing black cool pigments were conducted by a Scanning Electron Microscopy (SEM) (Zeiss LEO Supra 35VP SEMFEG) by using inLens and secondary scanning electron (SE2) modes and the electron voltage was kept constant at 5 kV. The working distance (WD) was kept between 5.4 – 6.9 mm. Before the SEM analysis, the samples were frozen in liquid nitrogen and then broken into half. The broken (fracture) surfaces were coated with gold and then analyzed under SEM. The distribution and the behavior of the pigments in the matrix were examined.

3.2.3.8. UV-vis-NIR Spectrophotometer

Surface light reflection from TPO samples with black cool pigments having dimensions as 16x16 cm were carried out by Cary 5000 UV VIS NIR Spectrophotometer at the range between 250-2500 nm with an accessory named Diffuse Reflection Accessory (DRA). The results were compared with the samples with carbon black and the titanium dioxide.

3.3. Results and Discussion

This section contains the results of the structural analysis of pigments and TPO sample characterization such as surface temperature, optical, physical, mechanical and thermal characterizations.

3.3.1. Pigment Analysis Results

Pigment analysis were done by XRF for metal and metal oxide content in pigments and by FTIR and NMR for structural content determination of organic transparent pigment. Also, laser diffraction system was used to determine the particle size of the both pigments.

XRF analysis results of pigments show that the reflective pigment contains significant amount of iron (Fe) and chrome (Cr) metals and their oxides since it has inorganic structure. However, transparent pigment, due to its organic structure, does not show any significant amount of metal or metal oxide but it also contains Ca and CaO which are so few in amount compared to inorganic content of reflective pigment that cannot be observable in the Figure 10a and 10b.

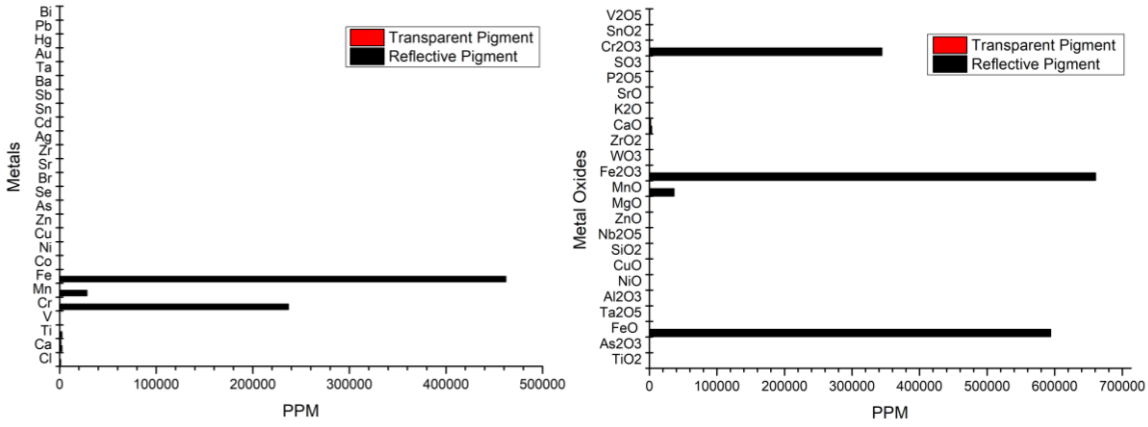

(a) **(b)**

Figure 10. XRF analysis of reflective and transparent pigment for (a) metal content (b) metal oxide content

FTIR analysis, represented in Figure 11, shows the perylene structure of transparent pigment and the functional groups that exists in the structure beside the perylene. The peaks around 1585 cm^{-1} corresponding at C=C stretching frequencies and the peaks around 3000 cm^{-1} and higher frequencies corresponding at aromatic C-H stretching are the significance of perylene structure. However, the peaks between 2800 – 2900 cm^{-1} corresponding to the C–H stretching of alky groups and the peaks around 1600 cm^{-1} corresponding to C=O in plane asymmetric stretching represents the existence of the functional groups [71]. These functional groups play a significant role in the fluorescence property of the perylene based pigments. Perylene contains cyclic structures with high optical stability due to its strong intermolecular π-π interactions between perylene cores. This strong interactions cause ordered 1D nanostructure and aggregates leading to fluorescence quenching called aggregation-caused quenching (ACQ). However, the substituent functional groups restrict the intermolecular π-π stacking between perylene cores and prevent the decrease of fluorescence intensity by fluorescence quenching. This results in fluorescence emission of the structure [72]. So, the transparent pigment used in this study, containing perylene structure with substituents as represented in Figure 9, has fluorescence property.

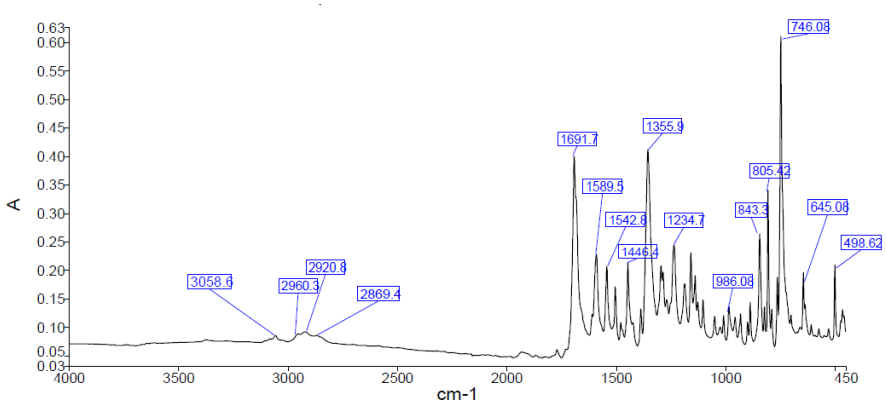

Figure 11. Determination of perylene structure and its substituents with FTIR analysis

Particle size analysis of pigments were conducted in order to observe the effect of particle size on reflectance behavior of pigments. According to Figure 12, reflective pigment has narrower particle size distribution peak with smaller particle sizes between 1 – 10 µm range. However, transparent pigment has wider 2 peaks between 1 – 10 µm range and for larger particles between 10 – 100 µm. The average of particle size (Dv(50)) for reflective pigment is 3.40 µm and for transparent pigment is 16.16 µm. Comparing to these black pigments, titanium dioxide contains two peaks; one of them being wider between 0.05 – 0.25 µm and the other is narrower around 1µm. It has an average of particle size Dv (50) of 1.005 µm. So, Figure 12 shows that reflective black pigment and titanium dioxide, being inorganic and containing metal oxides, have similar narrower particle size distribution with close values. However transparent pigment containing organic structure shows two wider peaks at higher particle size values.

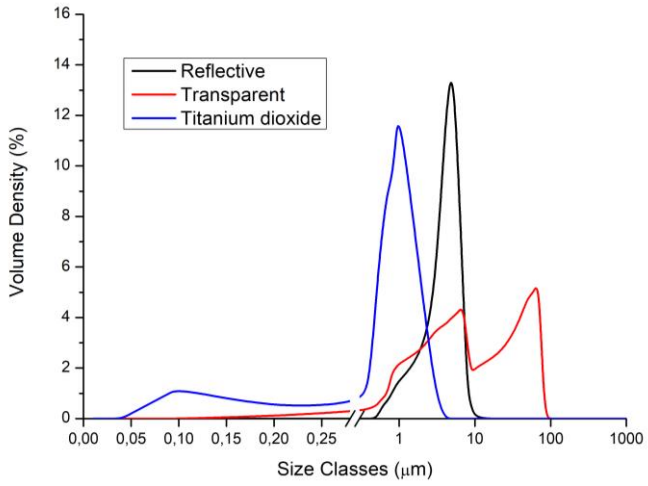

Figure 12. Particle size distribution of reflective and transparent pigments and TiO_2

3.3.2. TPO Sample Characterizations

TPO sample characterization contains the reflectance measurements and the surface temperature along with the mechanical and thermal characterizations.

3.3.2.1. Optical Characterization

Optical characterization of TPO compounds with cool black pigments, titanium dioxide and carbon black consist of their reflectance properties at UV-VIS-NIR region between 250-2500 nm as represented in Figure 13. The reflectance values for UV and visible (250-700 nm) range are same in all graphs where samples with reflective (REF) and transparent (TRANS) pigment and carbon black (CB) have nearly 0 values since they are black whereas the EMPTY sample and samples containing titanium dioxide (Ti) have higher reflectance values at this range. The exact difference between the samples become significant after 700 nm where the NIR region starts. 80% of the total energy in the NIR region arise from the 700–1300 nm wavelength region so, sunlight in this range plays the most important role in generating heat [73]. However, since reflectance values have inconsistency between the 800-950 nm wavelength due to the detector change of the device at this region, the accurate region for reflectance comparison is considered as between 1000-1300 nm.

Figure 13a, 13b and 13c represent the reflectance values of TPO samples with cool black pigments, titanium dioxide and carbon black comparing to empty sample at low, medium and high pigment loading, respectively. All these 3 graphs have the same trend such as the samples with reflective pigment (REF_1, REF_2, REF_3) have high and close reflectance values to samples with titanium dioxide (Ti_1, Ti_2, Ti_3) whereas samples with transparent pigment (TRANS_1, TRANS_2, TRANS_3) and samples with carbon black (CB_1, CB_2, CB_3) have very low reflectance values since they do not have reflective property. The EMPTY sample has an average value. This behavior can be explained with particle size of the incorporated reflective, transparent and titanium dioxide pigment. Since the absorption of light increases with increasing particle size, the particles having smaller size tend to have lower absorption and higher reflectance [74]. So, this can be considered as the reason for TPO compounds having reflective and titanium dioxide pigment, having small particle sizes according to Figure 12, show higher reflectance values whereas the TPO compounds with transparent pigment, having higher particle size, show low reflectance values. Also, comparing the reflectance values of

Figure 13a, 13b and 13c according to loading level, the reflectance values of samples with reflective pigment and titanium dioxide increases as the loading level increases. For instance, the sample containing reflective pigment at low loading level shows 47% reflectance at 1300 nm wavelength while this value increases up to 70% at high loading level. The same trend can be observed at samples with titanium dioxide where it has 64% reflectance value at low loading level but 90% reflectance at high loading level. So, it can be deduced that the reflectance increases with decreasing particle size of incorporated pigment and with increasing pigment content in the compound. Increasing pigment content even increases at the least the reflectance values of samples with transparent pigment.

Figure 13d and 13e represent the effect of increasing transparent and reflective pigment load on reflectance in mixed samples, respectively. In Figure 13d, the effect of increasing reflective pigment between samples MIX_2 (1%), MIX_3 (2%) and MIX_4 (3.67%) can clearly be observed at reflectance values which have an increasing trend such as 42%, 54% and 68%, respectively. Among them the reflectance value of MIX_4 mostly get close to the reflectance value of the sample containing titanium dioxide which has the highest reflectance value as 75%.

In Figure 13e, all samples named REF_2, MIX_1, MIX_3 and MIX_5 have same amount of reflective pigment (2%) with increasing transparent pigment loading of 0%, 0.1%, 0.2% and 0.4% respectively. At low and medium loading levels (0.1% and 0.2%) of mixed samples, the addition of transparent pigment decreases the reflectance value of the sample having only reflective pigment (REF_2) to 54% however transparent pigment addition at high loading level (0.4%), reaches the same reflectance value with REF_2 (64%). This behavior shows that since transparent pigment doesn't have reflective property, it is not effective on reflectance as much as reflective pigment.

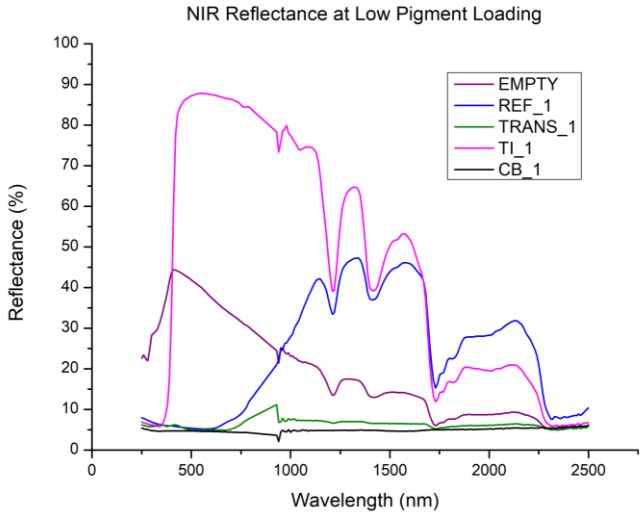
NIR Reflectance at Low Pigment Loading
Reflectance (%)
Wavelength (nm)
EMPTY
REF_1
TRANS_1
TI_1
CB_1

(a)

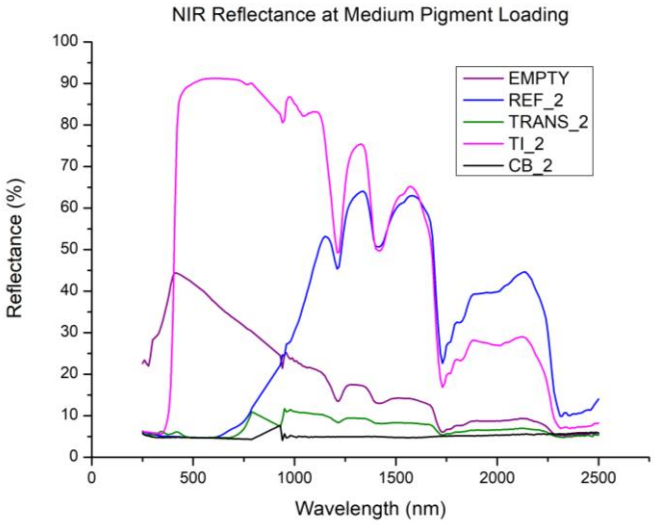
NIR Reflectance at Medium Pigment Loading
Reflectance (%)
Wavelength (nm)
EMPTY
REF_2
TRANS_2
TI_2
CB_2

(b)

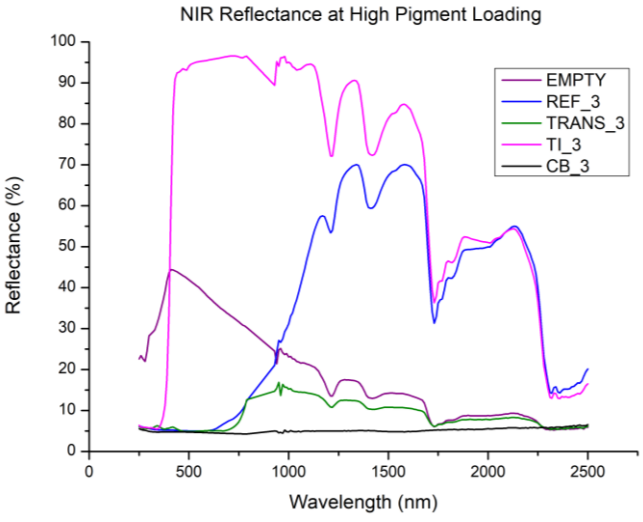
NIR Reflectance at High Pigment Loading
Reflectance (%)
Wavelength (nm)
EMPTY
REF_3
TRANS_3
TI_3
CB_3

(c)

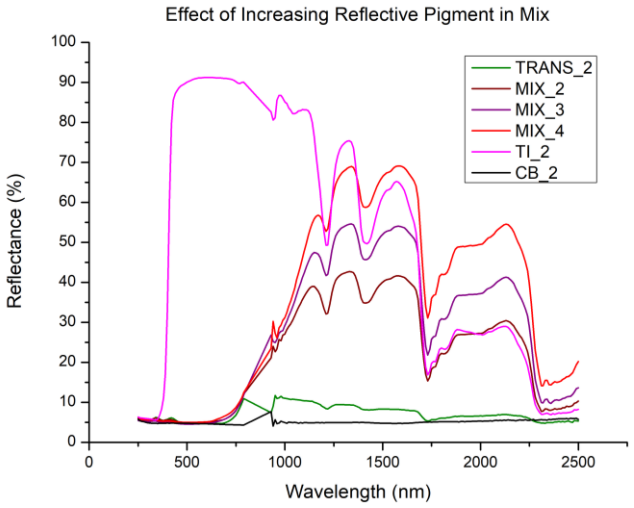

(d)

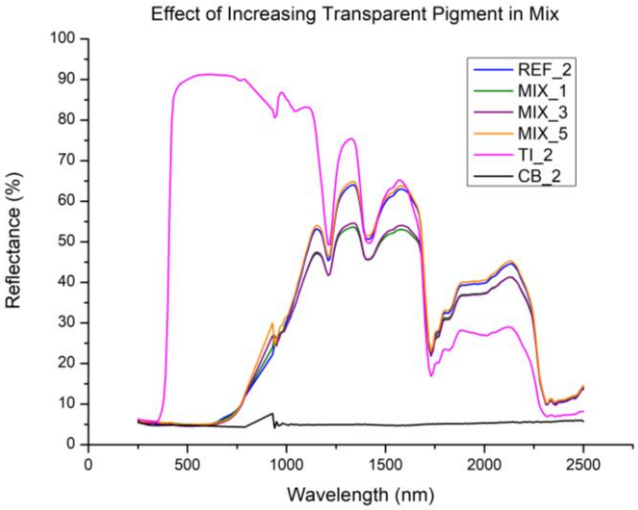

(e)

Figure 13. Reflectance values (%) of TPO samples with cool pigments, carbon black and titanium dioxide (a) at low pigment loading, (b) at medium pigment loading, (c) at high pigment loading, (d) with increasing reflective pigment loading in mix samples, (e) with increasing transparent pigment loading in mix samples

3.3.2.2. Surface Temperature Characterization

Surface temperature measurements show the temperature differences between the samples with conventional carbon black pigments, samples with cool black pigments and samples containing titanium dioxide pigment known as the coolest surface since it is white. These samples were also compared with the TPO sample without any filler or

pigment which is the base grade called “empty”. All graphs show that samples containing carbon black (CB_1, CB_2, CB_3) have highest values and any other pigment incorporation decreases the surface temperature increase.

Figure 14a to 14c represent the effect of pigment loading on the surface temperature increase of the samples within 3 hours timeline. Figure 14c, showing surface temperatures of samples with high pigment loading, has temperature values near and below 70℃ while Figure 14a and Figure 14b, showing surface temperatures of samples with medium and low pigment loading, respectively, have minimum temperature values above 70℃. So, the pigment loading effects the increase in surface temperature of TPO samples and increasing cool pigment amount in the compound decreases the surface temperature increase. Also, as seen in Figure 14a, 14b and 14c, at each pigment loading level, samples with reflective pigment (REF_1, REF_2, REF_3) have minimum or nearly minimum surface temperature values. At low pigment loading (Figure 14a) REF_1 has nearly the same surface temperature values with the compound containing titanium dioxide (Ti_1). However, at medium and high pigment loading (Figure 14b, Figure 14c) samples, containing reflective pigment, reach surface temperatures even lower than samples containing titanium dioxide and the empty sample despite they are white and colorless, respectively. So, it can be deduced that NIR reflective black pigment incorporation into TPO samples decreases the temperature of black surfaces even more than titanium dioxide.

Figure 14d represents the effect of increasing reflective pigment in mixed samples on surface temperature. TRANS_2 is considered as the sample without reflective pigment and MIX_2, MIX_3 and MIX_4 having increased reflective pigment content, respectively. Among these samples MIX_4 shows the lowest surface temperature containing highest reflective pigment with surface temperature between 70℃ - 75℃. On the other hand, Figure 14e represents the effect of increasing transparent pigment in mixed samples on surface temperature. Similarly, REF_2 is considered as the sample without transparent pigment and MIX_1, MIX_3 and MIX_5 having increased transparent pigment content, respectively. MIX_5, containing higher transparent pigment loading than others, has the lowest surface temperature. Also, comparing the two mix compounds having low surface temperature values (MIX_4 and MIX_5), MIX_5 has the lowest surface temperature which may considered as increasing transparent pigment content in mixture is more effective than increasing reflective pigment.

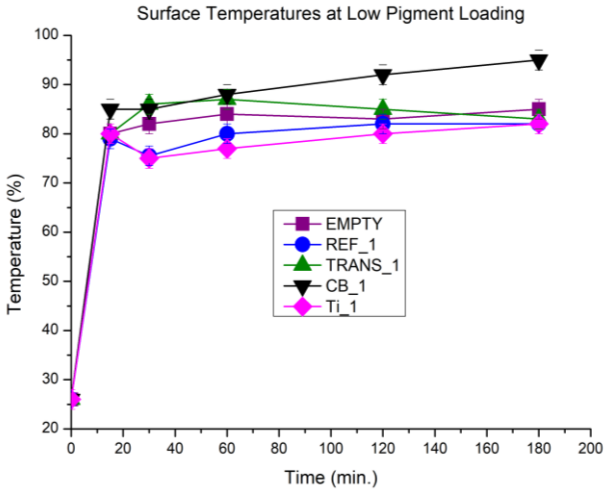
Surface Temperatures at Low Pigment Loading
Temperature (%)
Time (min.)
EMPTY
REF_1
TRANS_1
CB_1
Ti_1

(a)

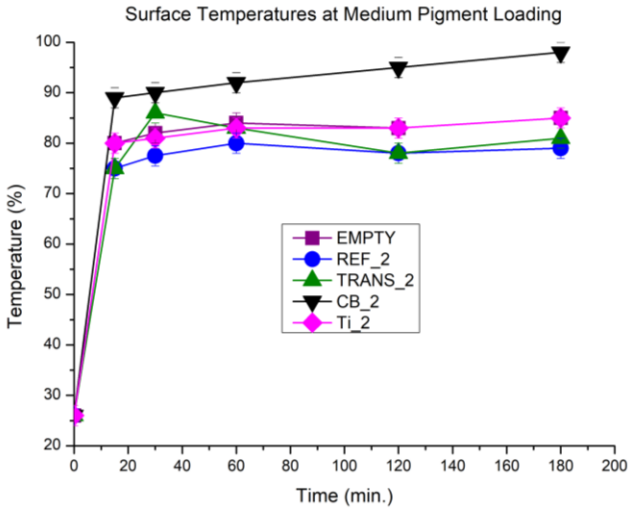
Surface Temperatures at Medium Pigment Loading
Temperature (%)
Time (min.)
EMPTY
REF_2
TRANS_2
CB_2
Ti_2

(b)

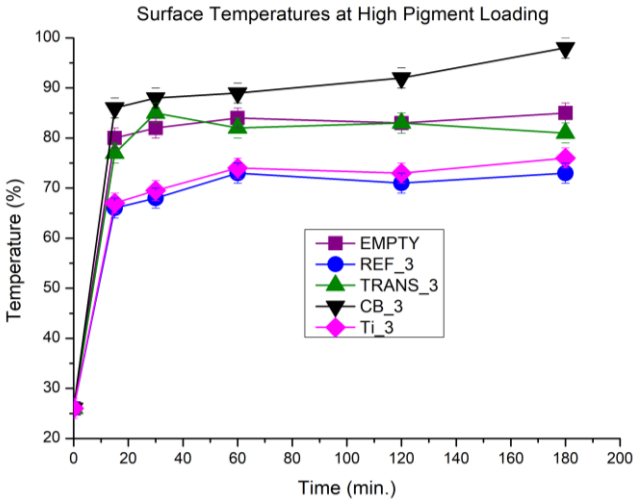
Surface Temperatures at High Pigment Loading
Temperature (%)
Time (min.)
EMPTY
REF_3
TRANS_3
CB_3
Ti_3

(c)

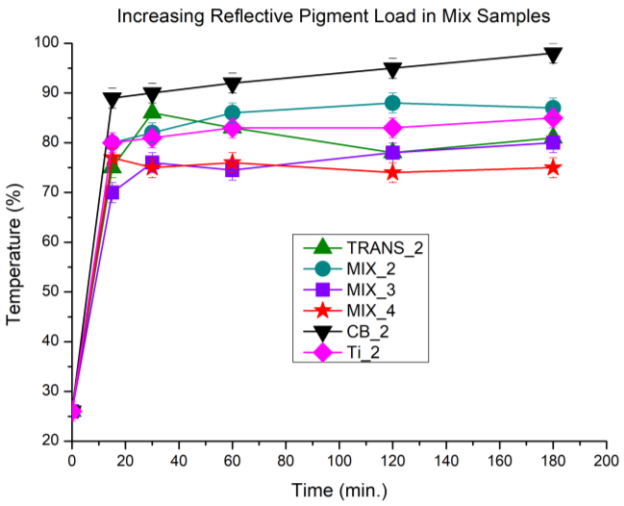

(d)

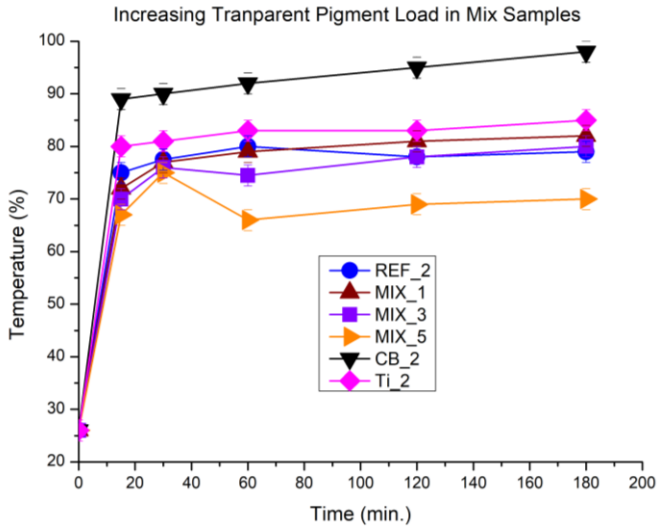

(e)

Figure 14. Temperature vs. time graph of TPO samples with cool pigments compared to TPO samples with conventional fillers, carbon black and titanium dioxide (a) at low pigment loading, (b) at medium pigment loading, (c) at high pigment loading, (d) with increasing reflective pigment load in mix samples, (e) with increasing transparent pigment loading in mix samples

Surface temperature of the of the samples reach nearly steady state at the end of 3 hours so these values are considered to be the optimum surface temperature values for comparison. Figure 15 represents the temperature change percentages samples with cool black pigments and samples with titanium dioxide with respect to samples with carbon black. According to Figure 15, samples with reflective pigment (REF_1, REF_2, REF_3) and with transparent pigment (TRANS_1, TRANS_2, TRANS_3) show an increasing trend in the surface temperature decrease with increasing pigment loading comparing to samples with carbon black. Also, in mixed samples, an increasing trend in surface temperature decrease can be observed between MIX_3 (2% reflective, 0.2% transparent), MIX_4 (3.67% reflective, 0.2% transparent) and MIX_5 (2% reflective, 0.4% transparent). The highest decrease is obtained with REF_3 (-25.5 %) and MIX_5 (-28.5 %) even having higher decrease values than the samples containing titanium dioxide, Ti_3, (-22.4 %). Since REF_3 has only 3,70% inorganic type filler (reflective pigment), whereas MIX_5 has 2% inorganic (reflective pigment) content and 0.4% organic (transparent pigment) content, MIX_5, having higher decrease in surface temperature than REF_3, ensures better performance with lower inorganic content.

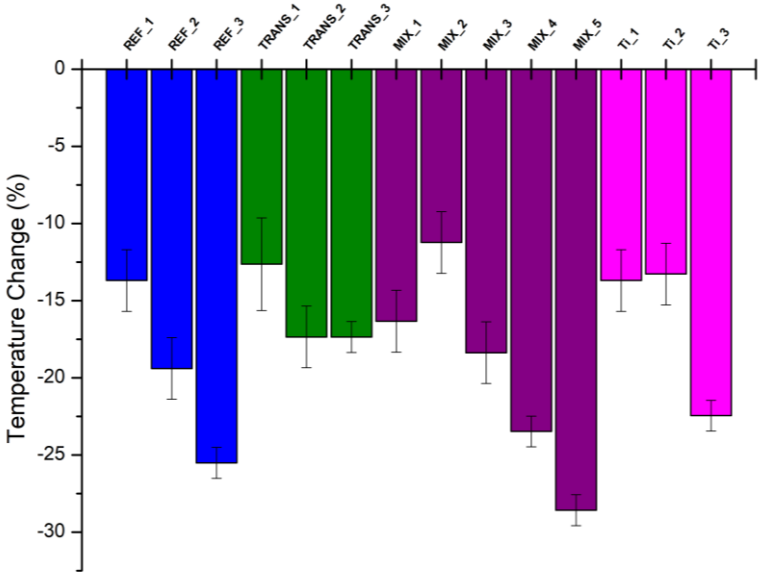

Figure 15. Temperature change (%) of TPO samples with cool pigments and titanium dioxide compared to TPO samples with carbon black after 3h under NIR lamp

3.3.2.3. Structural Characterization

Structural characterization of TPO samples involves analysis of the behavior of incorporated pigments in the PP matrix by SEM. These analysis were conducted from the fracture surface of TPO samples previously frozen with liquid nitrogen and broken into half.

Figure 16a shows the SEM image of the empty sample without any pigments whereas Figure 16b and 16c show the TPO samples loaded with reflective and transparent pigments respectively. In Figure 16b, the reflective pigments are obvious in the shape of particulates, well dispersed homogenously in the PP matrix and mostly in the form of agglomerates. However, in Figure 16c, transparent pigments are observed in the form of star-shaped structures at brighter locations. Since transparent pigment contains perylene structure which has fluorescent property, the regions with transparent pigments are seen brighter than the matrix [75].

Also, Figure 16d and 16e show the TPO compounds containing reflective and transparent pigments respectively, with closer view of agglomerated reflective pigments and fluorescent transparent pigments. Additionally, Figure 16f represents the mixture reflective and transparent pigments where agglomeration of the reflective pigments are marked with circles between the fluorescent perylene structures in PP matrix.

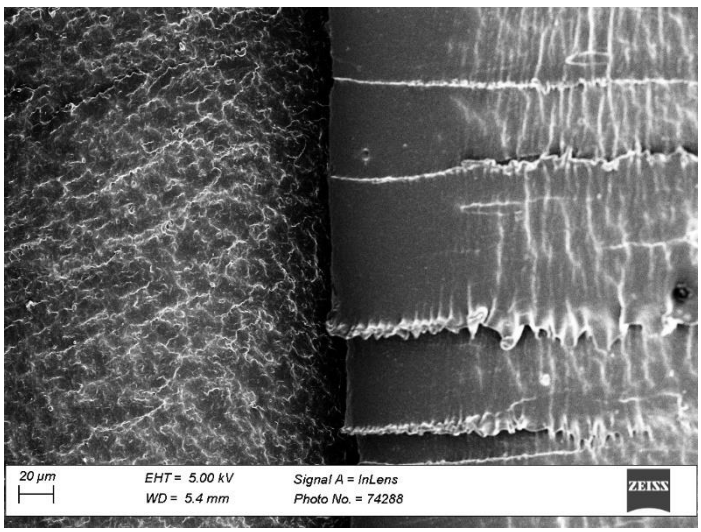

(a)

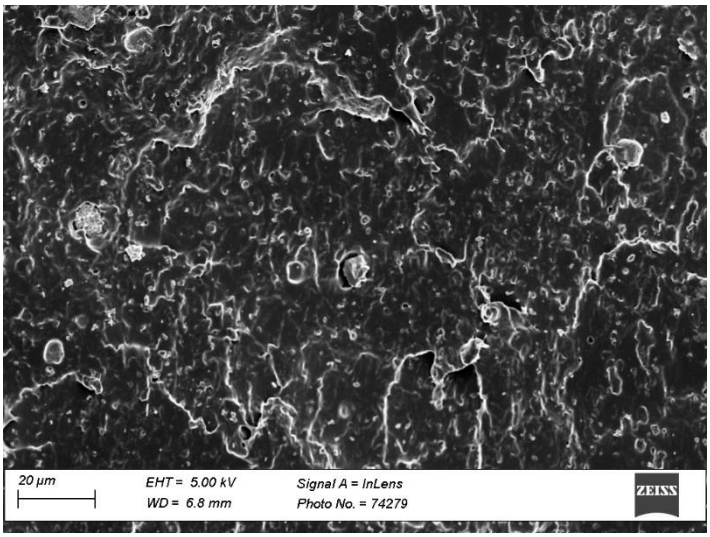
20 µm
EHT = 5.00 kV
WD = 6.8 mm
Signal A = InLens
Photo No. = 74279
ZEISS

(b)

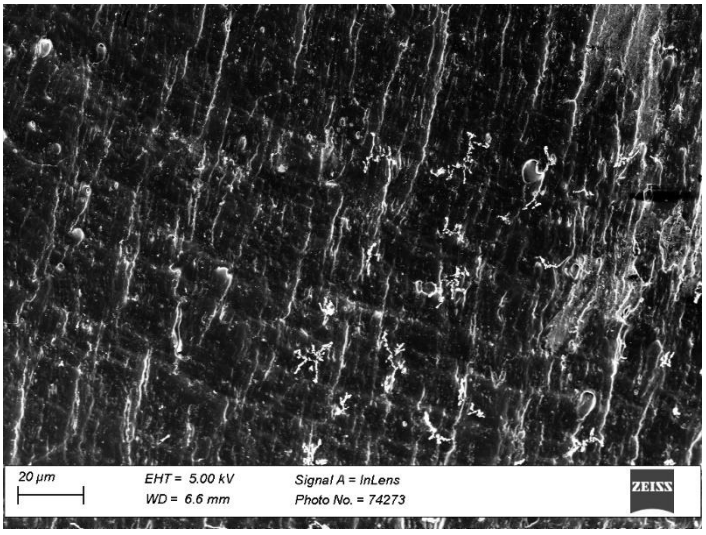
20 µm
EHT = 5.00 kV
WD = 6.6 mm
Signal A = InLens
Photo No. = 74273
ZEISS

(c)

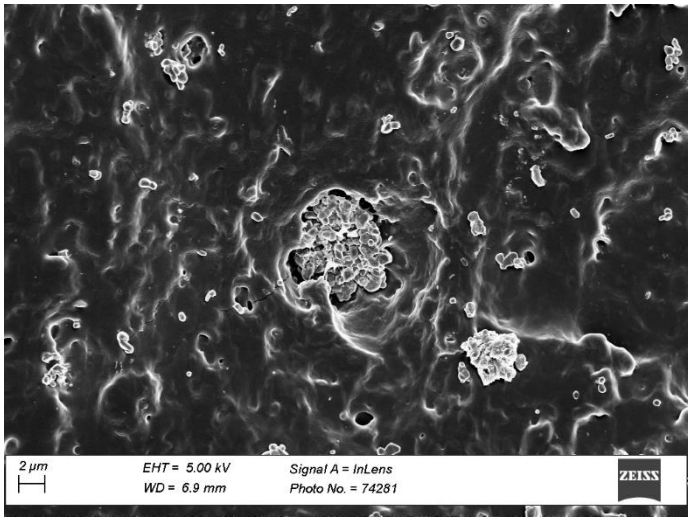
2 µm
EHT = 5.00 kV
WD = 6.9 mm
Signal A = InLens
Photo No. = 74281
ZEISS

(d)

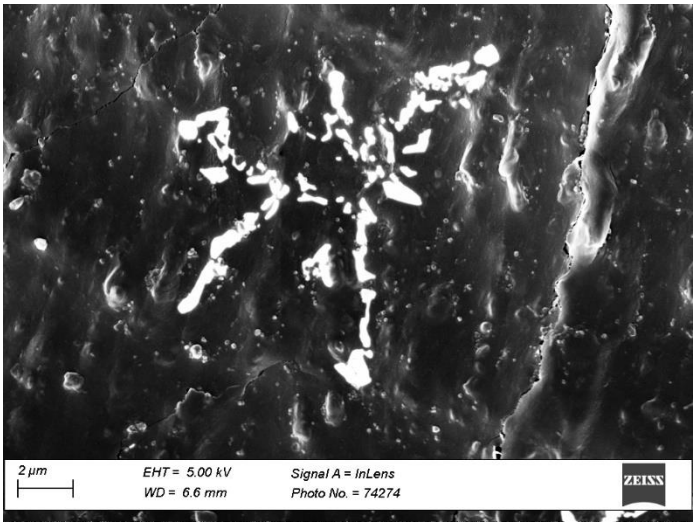

(e)

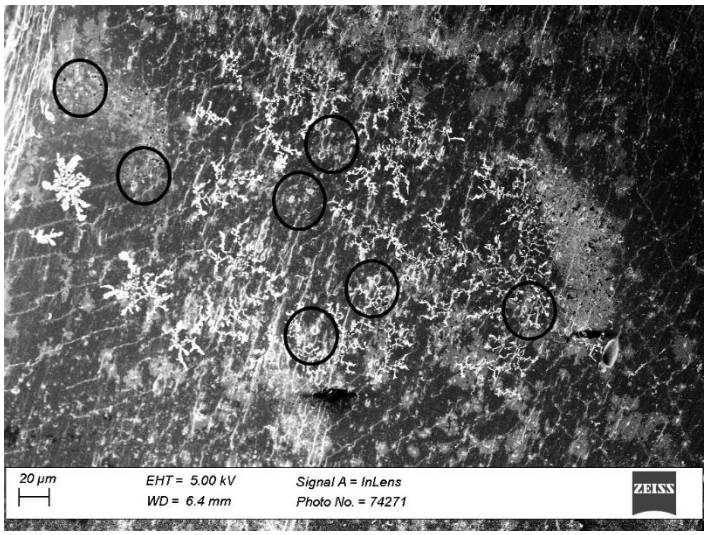

(f)

Figure 16. SEM images of TPO sample having a) no pigments (empty) at 800x magnification, b) reflective pigment at 1.75 kx magnification, c) transparent pigment at 1.50 kx magnification d) reflective pigment at 6 kx magnification e) transparent pigment at 13 kx magnification and f) mixture of reflective and transparent pigments at 681 magnification

3.3.2.4. Physical Characterization

Physical characterization of the TPO samples contains the mold shrinkage values at parallel and perpendicular directions to flow in Figure 17a and 17b respectively. According to Figure 17a, any type of pigment incorporation into “empty” sample increases the mold shrinkage value at parallel direction to flow. The addition of conventional pigments (carbon black and titanium dioxide) increases the mold shrinkage value at parallel direction, especially at high loading levels (CB_3 and Ti_3) more than the addition of cool black pigments (REF_, TRANS_, MIX_).

Increasing the loading level for each pigment group increases the mold shrinkage value. For instance increasing reflective pigment loading from REF_1 to REF_3 and increasing transparent pigment loading level from TRANS_1 to TRANS_3 increase the mold shrinkage values at parallel to flow direction. However, the effect of reflective pigment addition is more significant and show higher values when compared to addition of transparent pigment. This difference in the behavior can be stem from the behavior of the pigments in TPO compounds observed in SEM analysis. As represented in Figure 16b and 16d, the agglomerated structure of reflective pigments act as nucleating agent and cause an increase in the crystallinity of the TPO compound by functioning as driving force for crystallization rate acceleration. As the compound gets more crystalline with incorporation of reflective pigment which acts as nucleating agent, the mold shrinkage values also increase with increasing reflective pigment loading [76,77,78]. However, addition of transparent pigment does not contribute to increase in mold shrinkage value as reflective pigment. It also increases the mold shrinkage but less significantly.

A similar trend is also observed in mixed samples. The increasing reflective pigment content between samples MIX_2, MIX_3 and MIX_4 yields increasing mold shrinkage content due to nucleating agent property of inorganic reflective pigments whereas the increasing transparent content between MIX_1, MIX_3 and MIX_5 do not show a major increase in mold shrinakge values in parallel direction.

On the other hand, the mold shrinakge values at perpendicular to flow direction, in Figure 17b, show similar trend but with lower values. The addition of inorganic reflective pigment increases the mold shrinakge values whereas the addition of organic transparent pigment yields decrease in mold shrinakge values. Also, the mold shrinakge values of mixed samples show constant low values similar to the mold shrinkage values of

conpounds having transparent pigments. So, comparing the Figure 17a and 17b, one can deduce that the mold shrinkage is more obvious in parellel to flow direction due to flow induced crystallizaiton and agglomeration of reflective pigments.

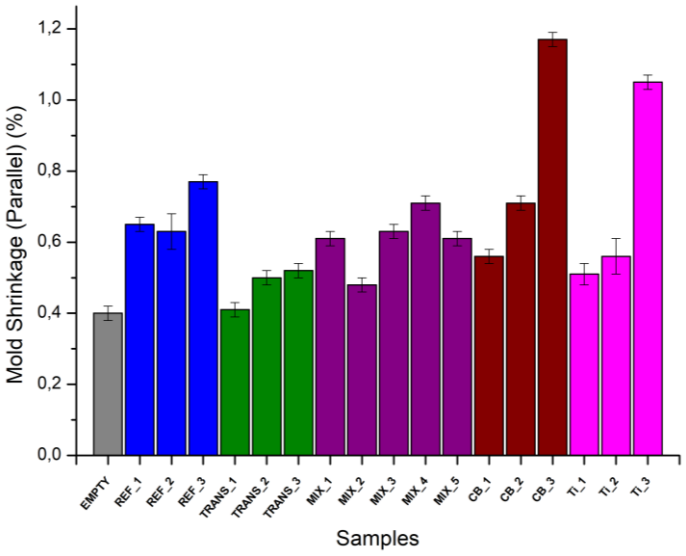

(a)

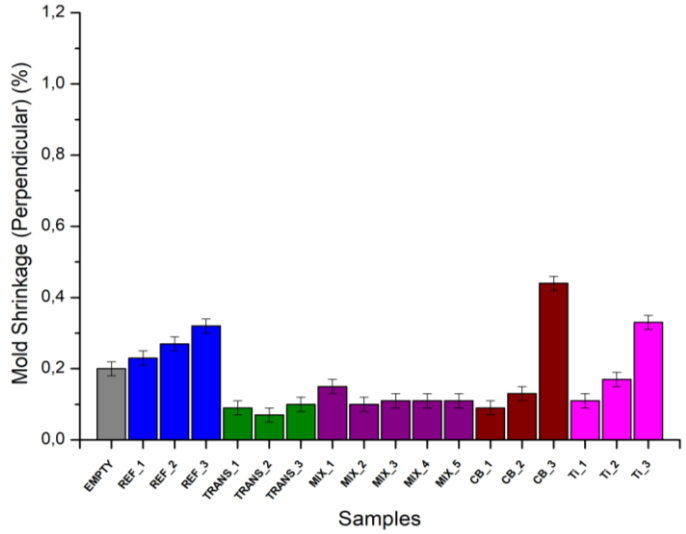

(b)

Figure 17. Mold shrinkage values of TPO samples with black cool pigments, conventional black pigments and titanium dioxide at a) parallel to flow direction b) perpendicular to flow direction

3.3.2.5. Mechanical Characterization

Mechanical characterization of TPO samples consist of tensile strength at break and elongation at break properties. According to 18a, any type of pigment incorporation like reflective and transparent pigment, carbon black and titanium dioxide increases tensile strength values. Similar to the mold shrinkage values, addition of reflective pigment is more effective than transparent pigment on increasing the tensile strength of the compound due to its nucleating agent property. The inorganic structures in the reflective pigment, acting as nucleating agents, provide large number of nuclei and accelerate the formation of crystalline regions so improve the tensile strength [79]. The effect of this behavior can also be observed in the MIX_ samples where the samples with higher reflective pigment loading show higher tensile strength value (MIX_4). The effect of pigment loading level is also significant for other samples. Increasing reflective pigment loading level between REF_1 to REF_3 and increasing transparent pigment loading level between TRANS_1 to TRANS_3 increases the tensile strength values. The samples with carbon black, which is the most commonly used filler to ameliorate the mechanical properties, show the highest tensile strength values at highest loading level. The high surface area property of carbon black prevents the dispersion of carbon black in PP matrix and creates a strong network structure with aggregates which yields higher mechanical properties [80]. As another inorganic filler, addition of titanium dioxide also increases the tensile strength values but it is not as significant as reflective pigment or carbon black.

Figure 18b represents the elongation at break values of TPO compounds. The addition of organic transparent pigment does not show a great effect on the elongation of compounds whereas addition of inorganic reflective pigment contributes to increase of elongation at break values. This behavior can also be explained with the nucleating agent behavior of the reflective pigment which may increase the toughness of the compound resulting in the increase of elongation at break values [81]. The mixed compounds show average elongation at break values between the values of compounds having only reflective and only transparent pigment since MIX_ compounds are composition of the pigments in definite ratios. However, commercial pigments, carbon black and titanium dioxide show different behaviors. While titanium dioxide has a little effect on elongation increase, addition of carbon black approximately doubles the elongation value of empty sample.

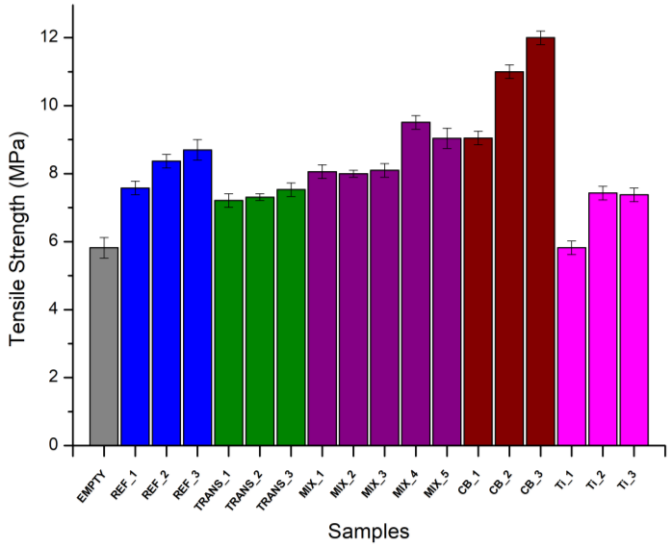

(a)

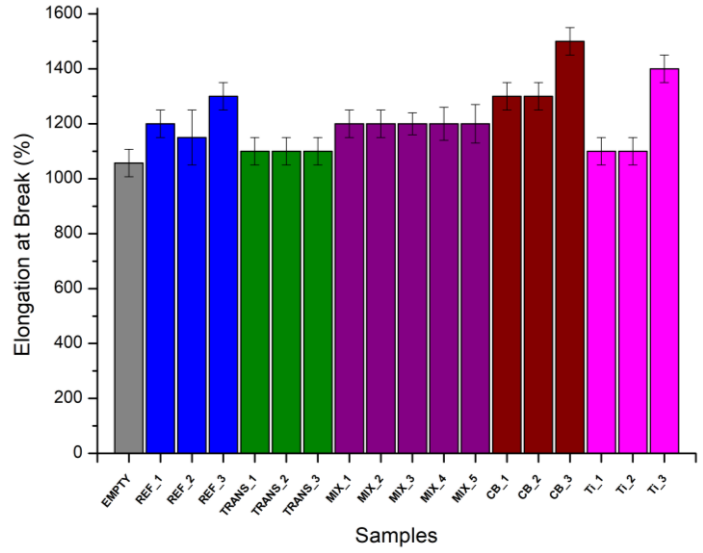

(b)

Figure 18. Effect of pigment incorporation into TPO samples on mechanical properties a) tensile strength b) elongation at break

3.4. Conclusion

This study was performed in order to investigate the effect of cool black pigment incorporation into TPO materials on surface temperature of these polymeric materials. For this purpose, two types of cool black pigments having NIR reflective property with inorganic structure and NIR transparent property with organic structure were chosen to be used in the TPO formulations and compared with the conventional pigments such as carbon black for its black color and titanium dioxide for its best NIR reflection property with white color. Also, samples containing mixture of the cool black pigments in certain loading levels were studied in order to observe the behavior of these pigments together in a compound.

Incorporation of these pigments in TPO materials resulted in different thermal and physical/mechanical properties of the final TPO products. Due to its reflective property, reflective pigment highly contributed to the decrease of the surface temperature with 25% temperature change comparing to carbon black. Even, at high loading level it cooled down the surface temperature more than titanium dioxide despite to its white color. However transparent pigment did not show a significant decrease on the surface temperature and remained limited only with 17% temperature change comparing to carbon black. While the surface temperature of the samples having carbon black reached around 100 ºC, the samples with reflective pigment it was managed to decrease this value around 70 ºC. The mixed samples also showed a considerable results. With constant transparent pigment loading, increasing reflective pigment loading between samples MIX_2, MIX_3 and MIX_4 showed a significant decrease on the surface temperature. However, with constant reflective pigment loading, increasing transparent pigment loading between samples MIX_1, MIX_3 and MIX_5 showed higher decrease on the surface temperature. In other words, increasing transparent pigment loading in mixed samples with constant reflective pigment content was more effective than increasing reflective pigment loading in mixed samples with constant transparent pigment content. According to these results, MIX_5 having 2% reflective pigment and 0.4% transparent pigment yielded the best surface temperature result with 28.2% surface temperature decrease and lower inorganic content comparing to samples with only reflective pigment.

Considering the physical and mechanical results, reflective pigment addition increased the mold shrinkage, tensile strength at break and elongation at break values by acting as

nucleating agent. However, transparent pigment was not as much effective as reflective pigment on physical and mechanical properties even it also slightly increased the values. So, optimum values for physical and mechanical results such as low mold shrinkage but high tensile strength and elongation at break values were obtained by MIX_ samples. Among the mixed samples, since the elongation at break values were same for all mixed samples, due to the highest reflective pigment content MIX_4 showed the best tensile strength results but also the highest mold shrinkage values which was not desirable. The lowest mold shrinkage values were obtained with MIX_2 but without sufficient mechanical properties and surface temperature decrease. So, when an optimum compound was intended with high tensile strength and elongation at break, low mold shrinkage value and low surface temperature with black color, MIX_5 was considered as the optimum TPO compound having 28.2% surface temperature decrease, 9.04 MPa tensile strength, 1200% elongation at break and with mold shrinkage values of 0.61% and 0.11% at directions parallel and perpendicular to flow respectively. In conclusion, this study showed that cool surface on black polymeric materials can be obtained with incorporation of pigments that prevent the absorption of light at NIR region and the physical and mechanical properties can be optimized by incorporation of these pigments in specific loading levels.

CHAPTER 4

4. Conclusion

This thesis study arose out of a series of environmental considerations such as changing climate due to increasing global warming which results in higher temperature increase in urban areas and excessive energy consumption by overuse of air conditioning. One of the areas that is highly affected from increasing temperature is vehicle indoors being exposed to sunlight for a long period of time in hot summer days. Due to that exposure, since the heat accumulated inside vehicles disrupts the comfort and the concentration of the driver, the need of a solution to get a cooler and comfortable environment inside the vehicle emerges. A possible solution for cooler vehicle indoor environment can be considered as decreasing the heat accumulated in the black polymeric parts in the vehicle instead of increasing the use of air-conditioning. For that purpose, an investigation of filler incorporation into the polymeric materials, used inside the vehicles, that decreases the heat accumulated in them by preventing the absorption of the sunlight that causes heat accumulation. Also, another problem arose from the production of the polymeric material, thermoplastic polyolefins (TPOs), commonly used in the inner black parts of the vehicles such as trim and dashboards, due to their better elastomeric properties. During the production of these TPOs, controlling their mold shrinkage is one of the most challenging problems since these parts have very high aspect ratio. A possible solution for this problem is considered as preparation of TPO compounds with low mold shrinkage. So, originating from these problems, this thesis treats these two problems and try to find an optimum combined solution. Primarily, it intends to create TPO materials having cool black surface with low mold shrinkage. In the light of this purpose, this thesis is composed of two major parts where the first part treats the generation of TPO formulations with low mold shrinkage and the second part investigates the incorporation of cool black pigment fillers into the TPO material with low mold shrinkage values in order to obtain cool black surface.

The first part of the study which was explained in chapter 2, treated the generation of TPO formulations and preparation of these TPO compounds intending low mold shrinkage. Considering the presence of the crystalline regions in a compound as the reason for mold shrinkage, in this study, the aim was to decrease crystalline regions and

increase the amorphous parts of the compound by incorporating plastomers which are known as more amorphous materials due to the presence of minor monomers such as octene or butene in their structure. For that purpose, in order to generate TPO compounds, four plastomers having different crystallinity values were chosen and incorporated into PP matrix in different loading levels as 30%, 50% and 70% and effect of incorporation of these plastomers on the final product and on their physical and mechanical properties were evaluated. Knowing that, the function and properties of final TPO product is highly dependent on the morphology and molecular structure of the incorporated plastomers, structural analysis of plastomers were also conducted by NMR and MD simulation. According to structural investigation of the plastomers, it was found that as the octene content in the structure increases, the plastomer forms a packed structure with less crystalline regions and get more amorphous. However, if the structure contains ethylene branching, the plastomer forms more extended structure, gets aligned and prone to crystallize. So, the results of the structural analysis showed that the plastomer having high octene content yields in low crystallinity value and the plastomer containing ethylene branching yields high crystallinity value. The incorporation of these low and high crystalline plastomers in TPO formulations affected directly the physical and mechanical properties of the TPO compounds. The lowest mold shrinkage values which are 0,02% and 0,09% at parallel and perpendicular to flow direction respectively, were obtained by incorporation of plastomer with lowest crystallinity (13%) at high loading level (70%) with compound C. However, since the mechanical properties of this compound was not high enough, the optimum compound was considered as compound A containing 70% plastomer with medium crystallinity and 30% copolymer PP because it showed low mold shrinkage values in parallel (0.19%) and perpendicular (0.2%) to flow direction and optimum tensile strength (13.4 MPa), tear strength (74.4 N/mm) and elongation at break (815%) results.

So, the findings of this study is useful in understanding the micro-events taking place during compound process of PP with plastomers, and to explain the necessary PP-plastomer ratio with desired mechanical traits.

The second part of the study which was explained in chapter 3, aimed to create cool surface on black polymeric materials by preventing the absorption of the part of the sunlight that causes heat accumulation which corresponds to NIR region. For that purpose, two types of pigment masterbatches which one of them contains NIR reflective

pigment which has property to reflect the light in the NIR region and the other contains NIR transparent pigment which has property to transmit the light in the NIR region were investigated. The reflective pigment having inorganic structure contained metal oxides and the transparent pigment having organic contained perylene structure. These pigments were incorporated into TPO sample C that was formulated in the first part of the thesis with lowest mold shrinkage values. These compounds with cool black pigments were compared with the compounds containing conventional pigments such as carbon black for its black color and titanium dioxide for its best NIR reflection property with white color. Also, compounds containing mixture of the cool black pigments in certain loading levels were studied in order to observe the behavior of these pigments together in a compound. The result of the pigment addition into TPO compound yielded thermal and physical/mechanical properties. Reflective pigment showed a significant decrease in the surface temperature of the compound with 25% temperature change comparing to carbon black. Even, at high loading level it cooled down the surface temperature more than titanium dioxide despite to its white color whereas transparent pigment addition was not effective enough to decrease the surface temperature of the compound and remained limited only with 17% temperature change comparing to carbon black. By the addition of reflective pigment, the surface temperature of compound with conventional carbon black pigment was managed to decreased from 100 ºC to 70 ºC. Additionally, compounds having both pigments as mixed samples also showed considerable result. Between the compounds having constant transparent pigment loading but increasing reflective pigment loading (samples MIX_2, MIX_3 and MIX_4), increasing reflective pigment showed a significant decrease on the surface temperature. On the other hand, between the compound having constant reflective pigment loading but increasing transparent pigment loading (samples MIX_1, MIX_3 and MIX_5) showed higher decrease on the surface temperature. In other word, in mixed state, increasing transparent pigment loading was more effective on decreasing surface temperature. So, according to these results, MIX_5 having 2% reflective pigment and 0.4% transparent pigment yielded the best surface temperature result with 28.2% surface temperature. Additionally, MIX_5 (2% reflective pigment + 0.40% transparent pigment) ensured higher decrease in surface temperature with lower inorganic reflective pigment content comparing to REF_3 (3.70% reflective pigment) which is the compound with highest inorganic pigment content and highest decrease in surface temperature among the compounds with only addition of one type of pigment. That is to say, preparation of mixed samples provided better surface temperature

performance (28.2% surface temperature decrease) with sample MIX_5, having lower inorganic content but higher decrease in surface temperature than REF_3 due to addition of organic transparent pigment.

When the physical and mechanical results were considered, mold shrinkage, tensile strength at break and elongation at break results showed that addition of reflective pigment encouraged the increase of the values due to its nucleating agent property whereas addition of transparent pigment was not as effective as reflective pigment. Although, the increase in tensile strength and elongation at break are favorable, the increase in mold shrinkage is not desired. So, the optimum results of mechanical properties and the mold shrinkage was obtained by mixed samples. Among the mixed samples, the highest mechanical results were obtained with MIX_4 but also had high mold shrinkage values. The best low mold shrinkage values were obtained with MIX_2 but without sufficient mechanical properties and surface temperature decrease. So, the optimum TPO compound with high tensile strength and elongation at break, low mold shrinkage value and low surface temperature with black color was considered as the sample MIX_5 having 28.2% surface temperature decrease, 9.04 MPa tensile strength, 1200% elongation at break and with mold shrinkage values of 0.61% and 0.11% at directions parallel and perpendicular to flow respectively.

In conclusion, this master thesis study managed to obtain TPO compound having cool surface on black polymeric materials by preventing the absorption of light at NIR region with desired mechanical properties and low mold shrinkage values.

References

1. Li C. Zhou J. Cao Y. Zhong J. Liu Y. Kang C. Tan Y. Interaction between urban microclimate and electric air-conditioning energy consumption during high temperature season. Applied Energy (117). (2014). p:149–156. http://dx.doi.org/10.1016/j.apenergy.2013.11.057
2. Randazzo T. De Cian E. Mistry M.N. Air conditioning and electricity expenditure: The role of climate intemperate countries. Economic Modelling (90). (2020). p:273–287. https://doi.org/10.1016/j.econmod.2020.05.001
3. Wenig C.L. Kau L.J. Design and Implementation of a Low-Energy-Consumption Air-Conditioning Control System for Smart Vehicle. Journal of Healthcare Engineering. (2019). https://doi.org/10.1155/2019/3858560
4. Subiantoro A. OOI K.T. Stimming U. Energy Saving Measures for Automotive Air Conditioning (AC) System in the Tropics. International Refrigeration and Air Conditioning Conference (Paper 1361). (2014). Available at http://docs.lib.purdue.edu/iracc/1361
5. Yang M.Q. Gao M. Hong M. Ho G.W. Visible-to-NIR Photon Harvesting: Progressive Engineering of Catalysts for Solar-Powered Environmental Purification and Fuel Production. Advanced Materials (30). (2018). https://doi.org/10.1002/adma.201802894.
6. Sun L. Liu X. Control Analysis of Production and Apparent Quality of Automobile Large Plastic Parts. Procedia Engineering (16). (2011). p.439-443. https://doi:10.1016/j.proeng.2011.08.1108
7. Sreedharan J. Jeevanantham A.K. Analysis of Shrinkages in ABS Injection Molding Parts for Automobile Applications / Materials Today: Proceedings (5). (2018). p:12744-12749. https://doi.org/10.1016/j.matpr.2018.02.258
8. MA Z.K. HUA L. SHI T.W. Study on the Instrument Panel Assembly Modal Analysis Basic on CAE Technology. Advances in Engineering Research (105). (2016). Available at (http://creativecommons.org/licenses/by-nc/4.0/
9. Warner, Darrel, E. et al. Thermoplastic Polymer Compositions and Method of Molding Parts with Reduced Shrinkage. (1996). World Patent WO 96/19533. Application Number: PCT/US95/16239.
10. Kaufman L. G. Et al. Thermoplastic Olefin Compositions. (2001). US Patent No.6,245,856 B1.

11. Brydson J.A. Thermoplastic Elastomers-Properties and Applications. (1995). p.13-22

12. Ito et al. Thermoplastic Olefin Elastomer Composition. (2004). US Patent No. 6,803,398 B1

13. Sun L. Liu X. Control Analysis of Production and Apparent Quality of Automobile Large Plastic Parts. (2011). p.439-443

14. Hennessey B. Ford Engineering Material Specification WSD-M2D381-A3. (2001)

15. Rodigas L. Ford Engineering Material Specification WSK-M4D550-A/A6. (2005)

16. Noh W.J. "Hyundai Material Specification, TPO Bumper Cover. (2008)

17. Shinde N.G. Patel D.M. A Short Review on Automobile Dashboard Materials. IOP Conference Series: Materials Science and Engineering. (2020). https://doi.org/10.1088/1757-899X/810/1/012033

18. Grestenberger G. Potter G.D. Grein C. Polypropylene/ethylene-propylene rubber (PP/EPR) blends for the automotive industry: Basic correlations between EPR-design and shrinkage. Express Polymer Letters. (2014). p.282–292. https://doi.org/10.3144/expresspolymlett.2014.31

19. Bhowmick A. K. Current Topics in Elastomer Research, Chapter 6: Plastomers. (2008). p.165

20. Lee H., Kim D.H., Son Y. Effect of Octene Content in Poly(ethylene-co-1-octene) on the Properties of Poly(propylene)/Poly(ethyleneco-1-octene) Blends. Journal of Applied Polymer Science. (2007). p.1133–1139. https://doi.org/10.1002/app.24644

21. Yamamoto T. Molecular dynamics of polymer crystallization revisited: Crystallization from the melt and the glass in longer polyethylene. The Journal of Chemical Physics. (2013). http://dx.doi.org/10.1063/1.4816707

22. Koyama A. Yamamoto T. Fukao K. Miyamoto Y. Molecular dynamics simulation of polymer crystallization from an oriented amorphous state. The American Physical Society. (2002). https://doi.org/10.1103/PhysRevE.65.050801

23. Avaz S. Oguz O. Kurt H. Menceloğlu Y.Z. Atılgan C. Soft segment length controls morphology of poly(ethylene oxide) based segmented poly(urethane-urea) copolymers in a binary solvent. Computational Materials Science. (2017). p.58-69. http://dx.doi.org/10.1016/j.commatsci.2017.06.018

24. Yang H. Zhao X.J. Li Z.S. Yan F.D. Molecular dynamics simulations on crystallization of polyethylene/fullerene nanocomposites. The Journal of Chemical Physics. (2009). https://doi.org/10.1063/1.3077864

25. Hafo Mould. Improve elastic properties & mechanical properties. Retrieved from https://hafo-mould.com/design-points-of-automobile-mold-making/

26. Dow Chemical Company ENGAGE™ Polyolefin Elastomers Product Selection Guide. (2004). Retrieved from https://www.avientdistribution.com/sites/default/files/0901b80380940420.pdf

27. Tesarikova A. Merinska D. Kalous J. Svoboda P. Ethylene-Octene Copolymers/Organoclay Nanocomposites: Preparation and Properties. Journal of Nanomaterials. (2016). http://dx.doi.org/10.1155/2016/6014064

28. Svoboda P. High-temperature study of radiation cross-linked ethylene–octene copolymers. Polymer Bulletin. (2017). p.121-144. https://doi.org/10.1007/s00289-016-1703-6

29. Dondero M. Pastor J.M. Carella J.M. Perez C.J. Adhesion Control for Injection Overmolding of Polypropylene with Elastomeric Ethylene Copolymers. Polymer Engineering and Science. (2009). p.1886-1893. https://doi.org/10.1002/pen.21415

30. ISO 37:2017, Rubber, vulcanized or thermoplastic — Determination of tensile stress-strain properties. BSI Standards Publication. (2017)

31. MaterialsStudio Materials Studio 6.0, Dassault Systems: San Diego. (2002)

32. Theodorou D.N. Suter U.W. Detailed molecular structure of a vinyl polymer glass. Macromolecules. (1985). p.1467–1478. https://doi.org/10.1021/ma00149a018

33. Sun H. COMPASS: an ab initio force-field optimized for condensed-phase applications overview with details on alkane and benzene compounds. The Journal of Physical Chemistry B. (1998). p.7338–7364. https://doi.org/10.1021/jp980939v

34. Andersen H.C. Molecular dynamics simulations at constant pressure and/or Temperature. The Journal of Chemical Physics. (1980). p.2384–2393. https://doi.org/10.1063/1.439486

35. Berendsen H.J.C. van Postma J.P.M. Vangunsteren W.F. Dinola A. Haak J.R. Molecular dynamics with coupling to an external bath. The Journal of Chemical Physics. (1984). p.3684–3690. http://dx.doi.org/10.1063/1.448118

36. Lobanov M.Y. Bogatyreva N.S. Galzitskaya O.V. Radius of Gyration as an Indicator of Protein Structure Compactness. Molecular Biology. (2008). p.701-706. https://doi.org/10.1134/S0026893308040195

37. Huggins M.L. The solubility of nonelectrolytes. By Joel H. Hildebrand and Robert S. Scott. The Journal of Chemical Physics. (1951). p.619–620.

38. Groot R.D. Madden T.J. Dynamic simulation of diblock copolymer microphase separation. The Journal of Chemical Physics. (1998). https://doi.org/10.1063/1.476300

39. Dee G.T. Sauer B.B. The cohesive energy density of polymers and its relationship to surface tension, bulk thermodynamic properties, and chain structure. Journal of Applied Polymer Science. (2016). https://doi.org/10.1002/app.44431

40. Simsek E. Oguz O. Bilge K. Çıtak M.K. Colak O. Menceloğlu Y.Z. Poly(propylene)/waste vulcanized ethylene-propylene-diene monomer (PP/WEPDM) blends prepared by high-shear thermo-kinetic mixer. Journal of Elastomers & Plastics. (2017). https://doi.org/10.1177/0095244317741759

41. Milczewska K. Voelkel A. The Use of Flory–Huggins Parameters as a Measure of Interactions in Polymer-Filler Systems. Journal of Polymer Science: Part B: Polymer Physics (44). (2006). p:1853–1862. https://doi.org/10.1002/polb.20843

42. LyondellBasell. Mold Shrinkage. p.1-2. Retrieved from https://www.lyondellbasell.com/globalassets/documents/polymers-technical-literature/tech-topic-mold-shrinkage.pdf

43. Chiang W.Y. Wu W.C. Pukanszky B. Modification of Polypropylene, Blending with Resole Type Phenol-Formaldehyde Resins. European Polymer Journal. (1994). p.573-580.

44. Balani K. Verma V. Agarwal A. Narayan R. Physical, Thermal and Mechanical Properties of Polymers. (2015). p.331-332.

45. Fujiyama M. Kimura S. Effect of Molecular Parameters on the Shrinkage of Injection-Molded Polypropylene. Journal of Applied Polymer Science. (1978). p.1225-1227. https://doi.org/10.1002/app.1978.070220506

46. Mieth F. Tromm M. Multicomponent Technologies. Specialized Injection Molding Techniques. (2016). p.1-51. https://doi.org/10.1016/B978-0-323-34100-4.00001-8

47. Kotek R. Afshari M. Harbisona V. Gupta A. Production methods for polyolefin fibers. Polyolefin Fibres. (2009). p.185-261. https://doi.org/10.1533/9781845695552.2.185

48. Gent A.N. Jeong J. Tear strength of oriented crystalline polymers. Journal of Materials Science. (1986). p.355-363.

49. Jose S. Aprem A.S. Francis B. Chandy M.C. Werner P. Alstaedt V. Thomas S. Phase morphology, crystallisation behaviour and mechanical properties of isotactic polypropylene/high density polyethylene blends. European Polymer Journal. (2004). p.2105-2115. https://doi.org/10.1016/j.eurpolymj.2004.02.026

50. Davisa L.W. Gertler P.J. Contribution of air conditioning adoption to future energy use under global warming. PNAS (19). (2015). p:5962-5967 www.pnas.org/cgi/doi/10.1073/pnas.1423558112

51. Wang N. Zhang J. Xia X. Energy consumption of air conditioners at different temperature set points. Energy and Buildings (65). (2013). p:412–418. http://dx.doi.org/10.1016/j.enbuild.2013.06.011

52. Fang V. Kenedy J. Futter J. Manning J. A review of infrared reflectance properties of metal oxide nanostructures. GNS Science Report (39). (2013). p:1-23.

53. Pisello A. L. High-albedo roof coatings for reducing building cooling needs. Eco-efficient Materials for Mitigating Building Cooling Needs. Elsevier. (2015). http://dx.doi.org/10.1016/B978-1-78242-380-5.00009-1

54. Coser E. Moritz V. F. Krenzinger A. Ferreira C. A. Development of paints with infrared radiation reflective properties. Polímeros. 25(3). (2015). p:305-310. http://dx.doi.org/10.1590/0104-1428.1869

55. Levinson R. Characterizing the Radiative Properties of Pigments for Cool Roofs. EETD Noon Seminar Presentation. (2004). Retrieved from https://coolcolors.lbl.gov/assets/docs/OtherTalks/Pigment-Talk-2004-04-22a.pdf

56. Rifdi Rizuan M. I. Abdul Wahab M. A. Romli A. Z. Effect of Carbon Black Structures towards Heat Build-up Measurements and Its Dynamic Properties. Advanced Materials Research (1134). (2015). p:131-137. http://dx.doi.org/10.4028/www.scientific.net/AMR.1134.131

57. Han D. Meng Z. Wu D. Zhang C. Zhu H. Thermal properties of carbon black aqueous nanofluids for solar absorption. Nanoscale Research Letters 6, 457. (2011). https://doi.org/10.1186/1556-276X-6-457

58. Dong S. Quek J.Y. Van Herk A.M. Jana S. Polymer-Encapsulated TiO2 for the Improvement of NIR Reflectance and Total Solar Reflectance of Cool Coatings. Industrial and Engineering Chemistry Research (59). (2020). p:17901−17910 https://dx.doi.org/10.1021/acs.iecr.0c03412

59. Jeevanandam P. Mulukutla R. S. Phillips M. Chaudhuri S. Erickson L.E. Klabunde K.J. Near Infrared Reflectance Properties of Metal Oxide Nanoparticles. Journal of Physical Chemistry C (111). (2007). p:1912-1918 https://doi.org/10.1021/jp066363o

60. Sangeetha S. Basha R. Sreerama K.J. Sangilimuthu S.N. Nair B.U. Functional pigments from chromium(III) oxide nanoparticles. Dyes and Pigments (94). (2012). p:548-552. https://doi.org/10.1016/j.dyepig.2012.03.019

61. Gonome H. Baneshi M. Okajima J. Komiya A. Maruyama S. Controlling the radiative properties of cool black-color coatings pigmented with CuO submicron particles. Journal of Quantitative Spectroscopy & Radiative Transfer (132). (2014). p:90–98. http://dx.doi.org/10.1016/j.jqsrt.2013.02.027

62. Kaur B. Quazi N. Ivanov I. Bhattacharya S.N. Near-infrared reflective properties of perylene derivatives. Dyes and Pigments (92). (2012). p:1108-1113. https://doi.org/10.1016/j.dyepig.2011.06.011

63. Wen T.C. Shetty D.K. Birefringence and Grain-Size Effects on Optical Transmittance of Polycrystalline Magnesium Fluoride. Proceedings of SPIE (7302). (2009). https://doi.org/10.1117/12.818933

64. Liang S. Zhang H. Luo M. Liu H. BAI Y. Xu H. Zhang Y. Preparation of Cr2O3-based pigments with high NIR reflectance via thermal decomposition of CrOOH. Transactions of Nonferrous Metals Society of China (25). (2015). p:2646−2652. https://doi.org/10.1016/S1003-6326(15)63887-0

65. Han A. Ye M. Zhao M. Liao J. Wu T. Crystal structure, chromatic and near-infrared reflective properties of iron doped YMnO3 compounds as colored cool pigments. Dyes and Pigments (99). (2013). p:527-530. http://dx.doi.org/10.1016/j.dyepig.2013.06.016

66. Levinson R. Berdahl P. Akbari H. Miller W. Joedicke I. Reilly J. Suzuki Y. Vondran M. Methods of creating solar-reflective nonwhite surfaces and their application to residential roofing materials. Solar Energy Materials & Solar Cells (91). (2007). p:304–314. https://doi.org/10.1016/j.solmat.2006.06.062

67. Kaur B. BHATTACHARYA S.N. Handbook of Textile and Industrial Dyeing || Automotive dyes and pigments. (2011). p:231–251. https://doi.org/doi:10.1533/9780857094919.2.231

68. Raj A.K.V. Rao P.P. Sameera S. Divya S. Pigments based on terbium-doped yttrium cerate with high NIR reflectance for cool roof and surface coating applications. Dyes and Pigments (122). (2015). p:116-125. http://dx.doi.org/10.1016/j.dyepig.2015.06.021

69. Mao Z. Yang Z. Zhang J. SrTiO3 as a new solar reflective pigment on the cooling property of PMMA ceramic composites. Ceramics International (45). (2019). p:16078–16087. https://doi.org/10.1016/j.ceramint.2019.05.124

70. Arunima S.R. Deepa M.J. Elias L. Aju Thara T.R. Geethanjali C.V. Shibli S.M.A. Tuning of surface characteristics of composite (WO3/BiVO4) zinc phosphate coatings

for industrial applications. Applied Surface Science (543). (2021). https://doi.org/10.1016/j.apsusc.2020.148822

71. Ganesamoorthy R. Sathiyan G. Thangamuthu R. Sakthivel P. Synthesis and Characterization of Bay Substituted Perylene Diimide Small Molecule for Organic Solar Cell Application. Springer Proceedings in Physics (189). (2017). https://doi.org/10.1007/978-3-319-44890-9_37

72. Zhang F. Ma Y. Chi Y. Yu H. Li Y. Jiang T. Wei X. Shi J. Self-assembly, optical and electrical properties of perylene diimide dyes bearing unsymmetrical substituents at bay position. Scientific Reports. (2018). https://doi.org/10.1038/s41598-018-26502-5

73. Oka R. Iwasaki S. Masui T. Improvement of near-infrared (NIR) reflectivity and black color tone by doping Zn^{2+} into the $Ca_2Mn_{0.85}Ti_{0.15}O_4$ structure. RSC Advances (9). (2019). https://doi.org/10.1039/c9ra07849e

74. Sun Z. Zhang J. Tong Z. Zhao Y. Particle size effects on the reflectance and negative polarization of light backscattered from natural surface particulate medium: Soil and sand. Journal of Quantitative Spectroscopy & Radiative Transfer (133). (2014) p:1–12. https://doi.org/10.1016/j.jqsrt.2013.03.013

75. Lee J.E. Stepanenko V. Yang J. Yoo H. Schlosser F. Bellinger D. Engels B. Scheblykin I.G. Würthner F. Kim D. Structure Property Relationship of Perylene Bisimide Macrocycles Probed by Atomic Force Microscopy and Single-Molecule Fluorescence Spectroscopy. ACS Nano (7). (2013). p:5064–5076. https://doi.org/10.1021/nn400616u

76. Wang S. Zhang J. Effect of nucleating agent on the crystallization behavior, crystal form and solar reflectance of polypropylene. Solar Energy Materials & Solar Cells (117). (2013). p:577–584. http://dx.doi.org/10.1016/j.solmat.2013.07.033

77. Xu T. Lei H. Xie C.S. The effect of nucleating agent on the crystalline morphology of polypropylene (PP). Materials and Design (24). (2003). p:227–230. https://doi.org/10.1016/S0261-3069(02)00129-2

78. Aliotta L. Cinelli P. Coltelli M.B. Righetti M.C. Gazzano M. Lazzeri A. Effect of nucleating agents on crystallinity and properties of poly (lactic acid) (PLA). European Polymer Journal Volume (93). (2017). p:822-832. https://doi.org/10.1016/j.eurpolymj.2017.04.041

79. Zhang X. Zhang D. Liu T. Influence of Nucleating Agent on Properties of Isotactic Polypropylene. Energy Procedia (17). (2012). p:1829 – 1835. https://doi.org/10.1016/j.egypro.2012.02.319

80. Al-maamori M.H. Al-Zubaidi A.A. Subeh A.A. Effect of Carbon Black on Mechanical and Physical Properties of Acrylonitrile Butadiene Rubber (NBR) Composite. Academic Research International (6). (2015).

81. Suksut B. Effect of Nucleating Agents on Properties of Natural Rubber Toughened Polylactic Acid. Suranaree University of Technology. (2009).